CENTRO DE INVESTIGACIONES EN ÓPTICA A.C.

Terahertz emission from spin polarization and relaxation in GaAs after optical orientation

Thesis presented by:

Jesús Alejandro Marín Calzada

Submitted in partial fulfillment of the requirements
for the degree of Master of Science (Optics).

Supervisor:
Dr. Enrique Castro Camus

October 30, 2013

Abstract

The terahertz (THz) band of the spectrum remained unexplored until recent years. New techniques and devices have been developed to analyze THz emission from several sources. THz emission spectroscopy opened a new window to study carrier dynamics in semiconductors with a temporal resolution of a few femtoseconds. This thesis presents a series of experiments to attempt to detect the THz radiation emitted when carriers are optically excited with circularly polarized light; since the optical orientation and spin relaxation transient is expected to emit a THz electric pulse. The theoretical basis of spintronics and the fundamental mechanisms involved during optical orientation and spin relaxation are presented in order to understand the mechanisms involved in spin transients. Semiconductors can generate THz radiation by a variety of processes that occur simultaneously depending on the semiconductor properties; and these effects are also explained. An initial proposal for the temporal profile of the THz radiation emitted by the changing magnetic moment is presented. The previous THz experiments leading to this thesis are also reviewed. The THz emission spectroscopy technique used for this thesis and the detection devices available to date are described. Finally, the experimental effort to find the spin THz emission is presented. The experimental setup is explained and the obtained measurements are studied. Power modulation of the pump beam, caused by the Liquid Crystal Retarder, was found and corrected for. The final measurement does not show the spin THz radiation, it is concluded that it might be smaller than expected.

A mis padres Ma. Alejandra y J. Jesús

A mi hermano Edgar Jair

I think nature's imagination is so much greater than man's that she's never going to let us relax.

Richard P. Feynman

Acknowledgments

I would like to thank the support of Consejo Nacional de Ciencia y Tecnología (México) for the scholarship that allowed me to take this masters degree program. Thanks to my supervisor Dr. Enrique Castro for his support during this research, for his patience and enthusiasm spreading knowledge to the students, and for his efforts as a science popularizer. Thanks to the members of my M.S. committee, Dr. Bernardo Mendoza and Dr. Miguel Vargas for their helpful career advice and suggestions in general.

Thanks to Dr. Ramón Carriles for his help with all the unexpected issues at the lab. Thanks to H. H. Tan, C. Jagadish and M. B. Johnston, for the substrates used to fabricate the photoconductive detectors described in Section 4.2.2. Thanks to Dr. Rafael for his useful advice with polarization issues. Thanks to Sofía for sharing with me her experience in the area, and to my friends of the THz group: Paulina, Monse, Ernesto and Adad.

Thanks to Centro de Investigaciones en Óptica (México) for showing me the way into the marvelous world of optics. Thanks to my buddies Omar, Daniel and Mike for the laughs. Thanks to Liliana Wilson for the great moments at the lab, for pushing my mind into the realm of imagination and future plans, but specially for teaching me the poetry of science. Thanks to my brother for being such a great engineer and a leading entrepreneur, which gives me a reason to be a good example and motivates us to compete for greater goals everytime. And finally, I want to thank my parents for all their unconditional love and support during all my life, for their trust in me for every challenge and most importantly for being the best parents.

Contents

1 Introduction **1**

1.1 The spin 2

1.2 Semiconductors 4

1.3 Objectives of this work 5

2 Spintronics **7**

2.1 Spin injection, transport and relaxation 8

2.2 Optical orientation 9

2.3 Spin relaxation 13

2.3.1 The Elliott-Yafet mechanism (EY) 14

2.3.2 The D'yakonov-Perel' mechanism (DP) 16

2.4 A comparison of spin relaxation mechanisms 19

2.5 Summary 20

3 Semiconductors as a source of THz radiation **23**

3.1 Optical rectification 24

3.2 Surge current 24

3.2.1 Built-in static electric field 25

3.2.2 Photo-Dember effect 26

3.3 Injecton and shift currents 26

3.4 Spin polarization and relaxation 27
3.4.1 Magnetic dipole radiation 27
3.4.2 Magnetic moment temporal evolution 28
3.5 A brief history of THz in semiconductors 31
3.6 Summary 36

4 THz spectroscopy 37
4.1 THz emission spectroscopy 38
4.2 THz detection 39
4.2.1 Free space electro-optic sampling 39
4.2.1.1 Polarization resolution limitations of FSEOS with (110) ZnTe 41
4.2.2 Photoconductive detection 41
4.2.2.1 Photoconductive detector alignment 44
4.3 Summary 45

5 THz emission spectroscopy of bulk GaAs 47
5.1 Experimental setup 47
5.2 THz radiation from optically excited bulk GaAs 50
5.3 Signal analysis 56
5.4 Summary 61

6 Conclusions 63
6.1 Further work 64

Chapter 1

Introduction

Electromagnetic waves are classified by their wavelength (λ), which is directly related to the energy of their photons by $E = hc/\lambda$. Typically, low frequency electromagnetic radiation is generated by charged particles (electrons) under acceleration, while high frequency radiation is produced by electron transitions from one quantum state to another. There is a spectral interval between these two regimes called the terahertz (THz) band, which had been unexplored until recent years. THz radiation, also known as far-infrared radiation, is defined between the frequencies from 300 GHz ($\lambda = 1$ mm) to 10 THz ($\lambda = 30\,\mu$m). THz radiation has been used to study protein dynamics [1], semiconductors [2] and superconductors [3], just to mention some applications. THz radiation has proven to be extremely useful to study the carrier dynamics in semiconductors [4].

Electronics is the branch of science that deals with the controlled flow of electrons. This technology has led to the creation of microprocessors which are used for information and signal processing. According to Moore's Law, micro-

processors will double in speed every 18 months, as technology advances and the size of electronic devices is reduced [5]. Yet, there is a physical limit when electronic devices reach the atom dimensions. Because of this, a new complementary science has emerged aiming to improve the functionality of electronics. Magnetoelectronics [6], also known as Spintronics, deals with a quantum property of electrons called *spin*. Spin polarization of electrons and holes can be used to transport information, but, in order to advance in the field of spintronics it is necessary to observe and manipulate both spins and currents in semiconductors [7].

The advances in THz detection and the scientific discoveries in the area of spintronics, can be used in combination to study the spin injection and spin relaxation dynamics in semiconductors. That is the purpose of this work, and the objective is to give a further step in spintronics development.

1.1 The spin

Spin is a purely quantum property of many particles such as electrons and holes. Every particle has its own spin, for example, the magnetic moment of a free electron is $\mu = -g\mu_B s/\hbar$, where μ_B is the Bohr magneton, $s = \hbar/2$, and $g = 2.0023$ is the free electron g factor. To achieve spin polarization in crystals, the average spin of a population of electrons must have a non-zero component [7]. In ferromagnetic metals the symbol $\uparrow$ ($\downarrow$) refers to carriers with magnetic moment parallel (antiparallel) to the magnetization, or as carriers with majority (minority) spin [7]. In semiconductors the term majority and minority refer to the relative population of the carrier, and $\uparrow$ (+) and $\downarrow$ (−) refer to the quantum numbers m_j with respect to the axis along the propagation of the excitation

laser beam. [8].

Spin can be transfered due to the interaction between particles and electromagnetic fields, hence the electron (hole) spin can be optically modified. An electromagnetic wave hitting an object can impart both energy and linear momentum to that object [9]. An electromagnetic wave transfers energy in quantized packets such that $E = \hbar\omega$, and the spin of a photon is either $+\hbar$ or $-\hbar$, where the signs correspond to the right or left handedness of circularly polarized light. The angular momentum of a photon does not depend on its energy [9].

A left-circularly (σ^-) polarized wave will impart angular momentum to the electrons because photons in the beam have their spins aligned in the direction of propagation indicated by the wave vector $\vec{\mathbf{k}}$. The injected magnetization is created in the same direction as the laser beam propagation. If the laser beam polarization changes from left circular to right circular (σ^+), the spin orientation of the photons is reversed [9], as shown in Fig. 1.1.

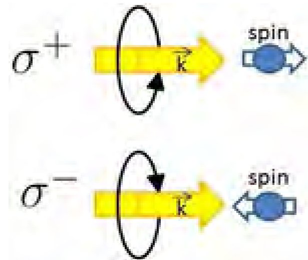

Figure 1.1: Induced spin by circularly polarized light

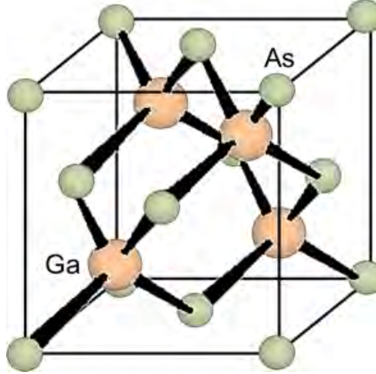

Figure 1.2: Zinc-Blende Structure of GaAs

1.2 Semiconductors

There is an intense search for highly spin polarizable materials suitable for spintronic device applications. The ideal case is where spins would be completely polarized even when no magnetic fields are present [7]. From the different types of materials, ferromagnets are the most commonly used in spintronics; half-metallic ferromagnets are predicted to have useful properties for spintronics, and finally, there is evidence for high spin polarization in III-V ferromagnetic semiconductors [7]. If spin polarizable semiconductors are available, this would facilitate the integration of traditional electronic and spintronic devices.

Inside the group of the III-V semiconductors, composed of elements from the groups III and V of the periodic table, metallic ferromagnetic semiconductors such as GaAs, show high spin polarization [7]. Gallium Arsenide (GaAs) is a III-V compound semiconductor with two different atoms. GaAs has a face-centered cubic unit cell. The crystal structure of GaAs is referred to as zinc-blende structure, since it is equivalent to ZnS [10], as shown in Fig. 1.2. The GaAs bandgap is $E_g = 1.424\,\text{eV}$ at a temperature $T = 294\,\text{K}$ and the spin split-off band is sep-

arated from the light and heavy hole bands by $\Delta_{so} = 0.34\,\mathrm{eV}$ [7]. GaAs is well know for its electronic and optical properties, and it is a good representative of the III-V zinc-blende semiconductors that will be used during the electronic and spintronic integration.

1.3 Objectives of this work

The goal of this thesis is to investigate the THz radiation emitted when carriers are optically excited with circularly polarized light. In order to identify the spin transient THz emission, all the mechanisms involved during the optical excitation need to be understood, and this thesis intends to describe the scientific basis required. Therefore, Chapter 2 presents a general review about spintronics from the optical point of view, and the physical processes that modify the spin polarization in semiconductors, such as spin injection, spin transport and spin relaxation. Chapter 3 presents several effects ocurring inside a semiconductor that generate THz radiation. It also shows how recent experiments are helping to clarify the photocarrier dynamics in semiconductors. In Chapter 4 the THz time-domain emission spectroscopy technique used to investigate the THz spin radiation is provided, as well as a brief review of a new polarization-sensitive THz detector. To verify the theoretical predictions, an experimental effort to understand the process of spin polarization/relaxation in GaAs after optical orientation is presented in Chapter 5 , where the experimental setup is described and the results are discussed. The conclusions and proposals for further work are presented in Chapter 6.

Chapter 2

Spintronics, the study of the carrier spin in solid state physics

The goal of spintronics is to understand the dynamics of spin with its surrounding environment, and to create useful devices using this knowledge. Fundamental studies still need to be done before spintronics could be used in real life applications. [7]. Spintronics is based on three fundamental processes: generation of carrier spin polarization(spin injection), spin polarized transport and spin relaxation.

The spin polarization or the nonequilibrium spin population, is achieved by some source of spin injection into the system that produces charge carriers with spin polarization [7]. Once the nonequilibrium spin population is created, a current of spin polarized carriers can be transported through the material. When the spin pumping is turned off, the spin will return to its equilibrium value due to carrier recombination and thermal spin relaxation.

2.1 Spin injection, transport and relaxation

A spin polarization can be produced by two methods: Electrical spin injection and Optical orientation. During the electrical spin injection, an unpolarized current is passed across a ferromagnetic semiconductor, and as it travels through it, the current becomes spin-polarized [11]. Electrical spin injection would also polarize nuclei and lead to a measurable effect in the electron spin resonance [7]. A second method for producing spin injection is Optical orientation, during which circularly polarized light transfers its angular momentum to electrons and holes creating spin polarized carriers [7]. Optical orientation is a non contact method that reduces the number of variables during the spin injection, so it offers some advantages over the electrical spin injection to analyze the photocarrier dynamics and its spin polarization and relaxation. The optical orientation method is of great interest for this work and will be discussed in detail in section 2.2.

Spin transport is basically the controlled motion of spin polarized carriers through a material. The spin transport relies on different conductivities for spin-up and spin-down electrons inside a nonmagnetic semiconductor [12] Spin transport differs from charge transport in that spin tends to relax to an equilibrium state, hence it is a non-conserved quantity in solids [7]. The basis for spin transport were established by Mott [13] who noticed an unusual resistance behavior in ferromagnetics metals at low temperatures. Mott noticed that, at these temperatures, electrons with magnetic moment parallel and antiparallel to the magnetization of a ferromagnet do not mix in the scattering processes [14]. The spin transport in III-V semiconductors such as GaAs has already been studied under these conditions [15]. Spin transport is an important subject for spintronics, but the present work is focused on the spin polarization and relax-

ation only, so transport will not be discussed any further.

Spin relaxation is a process by which spin equilibrium is restored. The electron spin relaxation time, in metals and semiconductors, oscillates around the nanosecond regime. Due to this relatively long life time, spin-encoded information can be sent through macroscopic distances, making spintronics a high potential technology [7]. The commonly used techniques that study the carriers spin usually neglect hole spin contributions because their lifetime is a lot shorter than the electron spin lifetime. But especially because of its short lifetime, 110 fs for heavy-holes [16], they may play an important role in ultrafast dynamics [17]. Spin relaxation is of great interest for this work and will be discussed in more detail in section 2.3.

2.2 Optical orientation

Optical orientation is the method by which circularly polarized light transfers its angular momentum to electrons and holes creating spin polarized carriers [7]. In 1968 Lampel [18] first demonstrated that optical spin orientation in silicon was possible when the interband absorption of circularly polarized light produced an appreciable spin orientation of the conduction band electrons. Three years later, D'yakonov and Perel' [19] gave a more detailed explanation about optical orientation. They explained that the electric field of a light wave acts directly on the orbital motion of the electron, but not on its spin. Therefore, spin orientation during interband absorption is produced by the spin-orbit interaction, which leads to a splitting of the valence band into the light and heavy holes bands and the so-called split-off band, as shown in Fig. 2.1. The energy dif-

ference between the top of the split-off band and the top of the light and heavy hole bands is Δ_{so}, which characterizes the magnitude of the spin-orbit coupling.

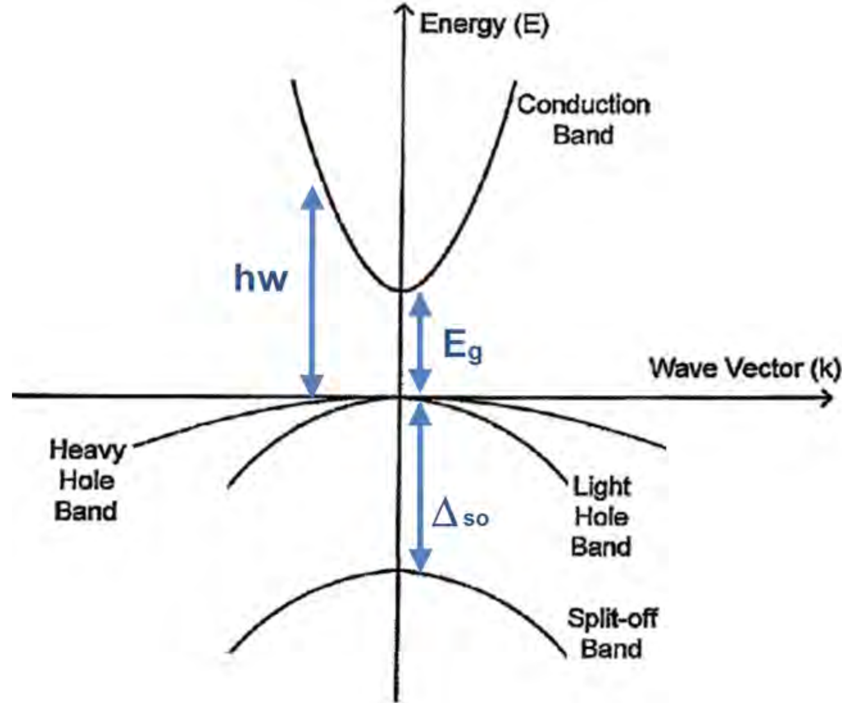

Figure 2.1: Splitting of the valence band into light and heavy holes bands, and the so-called split-off band.

In order to optically excite electron-hole pairs, it is known that the light energy $\hbar\omega$ must be greater than the bandgap energy E_g. After optically exciting carriers with circularly polarized light, the degree of spin polarization depends on the relation between $\hbar\omega - E_g$ and Δ_{so}. If $\hbar\omega - E_g \ll \Delta_{so}$, the electrons are excited into the conduction band from the valence band for which the spin-orbit coupling is large, and the degree of orientation counts to 50%. But if $\hbar\omega - E_g \gg \Delta_{so}$, then the spin-orbit interaction can be neglected, and the optical orientation of the electrons is null [19]. According to these rules, the relation $E_g \ll \hbar\omega \ll E_g + \Delta_{so}$ must be complied in order to produce spin

polarized carriers. As mentioned in Section 1.2, the bandgap energy for GaAs is $E_g = 1.42\,\mathrm{eV}$ and the spin-orbit splitting energy is $\Delta_{so} = 0.34\,\mathrm{eV}$, hence, the incident light energy for optical orientation in GaAs must be between 1.42 eV (870 nm) and 1.76 eV (705 nm).

The process of optical spin injection in a semiconductor with zinc-blende structure is as follows. Excitation with σ^+ polarized light produces two transitions: one that creates holes with a magnetic quantum of $m_h = 3/2$ and electrons with $m_e = -1/2$, the second transition produces holes with $m_h = 1/2$ and electrons with $m_e = 1/2$. In both cases the angular momentum is conserved since $m_h + m_e = 1$, which is the angular momentum of the photon. The relation between these two transitions is 3:1, which means that for every four photons, three $m_e = -1/2$ and one $m_e = 1/2$ electrons are created, and consequently, three ($m_h = 3/2$) heavy-holes and one ($m_h = 1/2$)light-hole appear [17], as shown in Fig. 2.2.

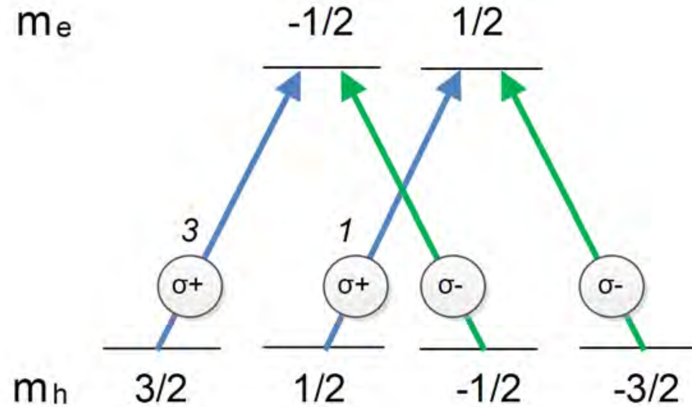

Figure 2.2: Spin transfer on electrons, heavy-holes and light-holes in zinc-blende semiconductors

The efficiency of the optical spin injection can be described by the spin polarization of the carrier density [7]. Spin polarization in general (on electrons, holes, nuclei) can be defined as

$$P_X = \frac{X_+ - X_-}{X_+ + X_-} \tag{2.1}$$

where X_+ and X_- are the spin components for a particular quantity X. Defining n_+ and n_- as the electron density parallel ($m_e = 1/2$) and antiparallel ($m_e = -1/2$) to the direction of the light propagation respectively, the electron spin polarization can be found as

$$P_n = \frac{n_+ - n_-}{n_+ + n_-} \tag{2.2}$$

For a zinc-blende structure, $P_n = (1-3)/(1+3) = -1/2$ is the electron spin polarization at the moment of photoexcitation. A reversal in the circular polarization of light, will cause a sign reversal of the electron density polarization [7]. In bulk III-V semiconductors, GaAs for example, optical orientation can lead to 50% polarization of electron density [7]. The degree of spin polarization in semiconductors has been theoretically studied by B. S. Mendoza [20]. On the experimental side, J. G. Braden *et al.* have measured directly the degree of spin polarization on the magnetic semiconductor (Ga,Mn)As using Andreev reflection spectroscopy [21]. The electron spin polarization has been presented here, but the same formula applies for holes which should not be forgotten. Furthermore, holes in a semiconductor can have larger magnetic moments than electrons, therefore, they can make larger contributions to the optical spin injection [17].

2.3 Spin relaxation

Spin relaxation is the process by which spin polarized carriers return to the spin equilibrium. The spin density will decrease exponentially with the inverse time constant $1/T_s = 1/\tau + 1/\tau_s$, where τ_s is the spin relaxation time and τ is the carrier lifetime [19]. In the valence band the hole spin relaxes rapidly, but the spin relaxation time of the electrons in the conduction band may exceed their lifetime. If the spin survives the carrier recombination $\tau < \tau_s$, there will be a recombination radiation with spin information [19]. The recombination radiation will be circularly polarized with the same kind of circular polarization as the exciting light. However, the electron spin relaxation times, in metals and semiconductors, oscillates around the nanosecond regime [7], so they are not under the focus of this work.

Spin relaxation occurs in electrons and holes, and the later lose their spin in a shorter period of time. The hole spin relaxation plays a direct role in electron-hole exchange interactions [16], therefore, understanding the hole spin relaxation will help for a better understanding of the electron spin relaxation process as well. The hole spin relaxation time has already been studied by Hilton and Tang [16]. Using time and polarization resolved femtosecond spectroscopy, they found the spin relaxation time of heavy holes in bulk GaAs to be 110 $\pm$10% fs.

In metals and semiconductors, there are four mechanisms by which the carrier spin relaxes: the Elliott-Yafet, D'yakonov-Perel', Bir-Aronov-Pikus, and hyperfine-interaction mechanisms [7]. The Elliott-Yafet mechanism is caused by the spin-orbit coupling induced by ions. The D'yakonov-Perel' mechanism is caused by the spin dephasing in noncentrosymmetric solids, where the lack of symmetry exerts an effective magnetic field into the carriers. The Bir-Aronov-

Pikus mechanisms plays an important role in p-doped semiconductors, where electron-hole exchange interaction gives rise to fluctuating local magnetic fields that flipp carrier spins. Finally, the hyperfine-interaction mechanism dominates the spin dephasing of localized or confined carrier spins in semiconductor heterostructures such as quantum wells and quantum dots [7]. Only the first two mechanisms apply for bulk GaAs and they will be discussed in detail in Sections 2.3.1 and 2.3.2 respectively.

2.3.1 The Elliott-Yafet mechanism (EY)

Overhauser [22] first studied the spin-lattice relaxation on free electrons using various mechanisms. He obtained times somewhat longer than those observed in alkali metals, but his effort was a milestone for Elliot's and Yafet's work. Elliot was the first to realize that conduction electron spins can relax via ordinary momentum scattering (such as by phonons or impurities) if the lattice ions induce spin-orbit coupling in the electron wave function [7]. Elliot [23] developed a theory to understand some magnetic resonance effects in impurity semiconductors taking into account the spin-orbit coupling effects. He started introducing the appropriate spin-orbit interaction into Schrödinger equation by expanding the potential V with the four-component Dirac equation and then reducing it to two components so that the spin-orbit coupling is taken into account. Then he developed an expression for the spin orbit coupling by means of an approximation considering that almost all the spin-orbit interaction arises when the electron is close to the nucleus and that external fields have little effect.

Yafet [24] also analyzed the spin-orbit interactions in a more complete work where he presented the spin orbit coupling, the spin-lattice relaxation in nonde-

generate bands, the g factor theory and its respective comparison with experimental results. He stated that the spin-orbit interaction is the most important mechanism that couples the spin moment to the orbital motion, and it determines the g factor and the spin lattice relaxation time. The spin-orbit coupling alone does not lead to spin relaxation, however, in combination with momentum scattering, the spin-up and spin-down states can couple and lead to spin relaxation [7].

Yafet [24] explained that, in the literature on paramagnetic resonance, the g factor, defined as an experimentally measured quantity, relates the frequency ν of resonance to an applied magnetic field H as: $h\nu = g\beta H$, where β is the Bohr magneton. Similarly, Elliot [23] states that the Hamiltonian of the interaction between a magnetic field and an electron is $\beta\mathbf{H} \cdot (\mathbf{l} + 2\mathbf{s})$. But the twofold degeneracy of the electron states causes a splitting called $g\beta H$ where g is defined as a matrix element of $2(\mathbf{l} + 2\mathbf{s})$, and depends on the direction of $\mathbf{H}$ and on $\mathbf{k}$. He computes the value of g in three cases which seem to cover the possible band forms:

A. Electrons in a nondegenerative band

B. Electrons with kinetic energies large compared to the spin-orbit coupling energy occupying states with energies near a point where bands are degenerate.

C. Electrons in a degenerate band with energies small compared to the spin-orbit coupling

After many calculations, and thanks to some crude approximations, for the three cases stated above, he found a formula for the relaxation time by lattice

scattering in semiconductors:

$$\tau_S \sim \frac{\tau_R}{(g-2)^2} \tag{2.3}$$

where τ_R is the relaxation time characteristic of electrical resistivity.

He also got some equations for the relaxation time by impurity scattering in semiconductors. For the case A, below the Fermi temperature

$$\tau_S \sim \frac{\tau_R}{(g-2)^2 c^{\frac{2}{3}}} \tag{2.4}$$

where c is the concentration of the impurities.

For the case A, above the Fermi temperature

$$\tau_S \sim \tau_R[\hbar^2/2mkT(g-2)^2 a_0^2] \tag{2.5}$$

where a_0 is the atomic radius, k is the magnitude of the wave vector and T is the temperature in K.

For the case B

$$\tau_S \sim \frac{\tau_R}{(g-2)^2} \tag{2.6}$$

And finally, for the case C

$$\tau_S \sim \tau_R \tag{2.7}$$

2.3.2 The D'yakonov-Perel' mechanism (DP)

D'yakonov and Perel' [25] found a spin relaxation mechanism produced by spin-orbit splitting of the conduction band in systems lacking inversion symmetry. The band splitting is proportional to the cube of the quasimomentum, which is

a momentum-like vector associated with electrons in a crystal lattice. The band splitting also increases rapidly with increasing electron energy [19]. The spin splitting of the conduction band is equivalent to a magnetic field acting on the spins [25]. Most of the materials without inversion symmetry come from groups III-V (such as GaAs) and II-VI semiconductors, where inversion symmetry is broken by the presence of two distinct atoms in the Bravais lattice [7]. The main feature of this mechanism is that the purer the crystal and the greater the elctron energy, the more effective the mechanism. This mechanism is important for hot electrons, specially those high in the conduction band [25].

Because of the presence of a spin splitting of the conduction band in such crystals, the energy of the electron depends on the spin component in the direction of the vector $\vec{\mathbf{k}}$ which is related to the momentum [25]. The energy splitting can be written as:

$$\hbar\Omega = 2\alpha k(2m_c)^{-3/2}E_g^{-1/2} \tag{2.8}$$

where α is a certain numerical coefficient, m_c is the electron mass in the conduction band and Ω is the precession frequency of the spin in a certain effective magnetic field directed along $\vec{\mathbf{k}}$. If the electron spin makes certain angle with the vector $\vec{\mathbf{k}}$ at the first instant, there will be a precession of the spin around $\vec{\mathbf{k}}$ at a frequency Ω. Scattering produces a change in the momentum of the electron which leads to a rotation of the axis of precession. Therefore, the original existing orientation of the spin will relax [19].

Unlike the Elliot-Yafet mechanism which involves spin rotation during col-

lisions, the D'yakonov-Perel mechanism is effective in the intervals between collisions. If there were no collisions, this mechanism will produce an inhomogeneous spin population analogous to random local magnetic fields. In the intervals between collisions the spin of each electron processes about the direction of the effective magnetic field which defines the direction of the quasimomentum. Then, collisions change the momentum of the electron and rotate the precession axis. If the time between collisions is less than the precession period, then the electron spin will not be able to follow the frequent rotations of the precession axis and the effect of the spin-orbital splitting will be substantially suppressed [25]. Under these conditions spin relaxation time is of the order of $(\Omega^2 \tau_p){-}1$, where Ω is the precession frequency and τ_p is the momentum relaxation time.

It was found that [25], the spin relaxation time in semiconductors without degeneracy is given by:

$$\frac{1}{\tau_s} = b\alpha^2 \frac{\tau_p T^3}{h^2 E_g} \tag{2.9}$$

where b is a degeneracy dependent constant. And the spin relaxation time in semiconductors in the presence of degeneracy is given by:

$$\frac{1}{\tau_s} = b\alpha^2 \frac{\zeta^3 \tau_p(\zeta)}{h^2 E_g} \tag{2.10}$$

where ζ is the electron concentration.

2.4 A comparison of spin relaxation mechanisms

The most important difference between the Elliott-Yafet and the D'yakonov-Perel' mechanisms is their opposite dependence on τ_p. While increased scattering intensity makes the Elliott-Yafet mechanism more effective, it decreases the effectiveness of the D'yakonov-Perel' processes; this has been experimentally demonstrated by Z. G. Yu and S. Krishnamurthy [26]. Their study was limited to the Elliot-Yafet and the D'yakonov-Perel' mechanisms, and they demonstrated that D'yakonov-Perel' mechanism does not contribute to spin relaxation of heavy holes as that would require spin precession from $m_h = \pm 3/2$ to $m_h = \mp 3/2$, which is forbidden because $|\delta m_h| > 1$, therefore, the Elliot-Yafet mechanism is the sole origin for the heavy-hole spin relaxation and the dominant one for the light-hole spin relaxation. On the other hand, for electrons, the Elliot-Yafet mechanism is important only at very low energies ($\leq 30\,\mathrm{meV}$) and D'yakonov-Perel' dominates at higher energies [26].

An equation was also developed by Z. G. Yu and S. Krishnamurthy [26] to enable a direct computation of the carrier spin lifetimes from accurate electronic structures. They presented the calculated electron and hole spin relaxation times as a function of the photon energy at room temperature [26]. Their proposed theory to understand the different spin relaxation times between carriers states that: *"The much shorter spin relaxation times of holes than those of electrons can be understood by noticing that in any state of the light-hole and the split-off bands, up-spin and down-spin are strongly mixed, which is in sharp contrast to the situation of conduction-band states, where the mixture between*

up-spin and down-spin is usually very small. Thus when a heavy hole scatters into a light-hole state or vice versa, a significant amount of spin will flip, giving rise to very fast spin relaxation." [26].

2.5 Summary

The three fundamental processes for spintronics: spin injection, spin transport and spin relaxation have been presented. Spin injection can be achieved by electrical injection and optical orientation. Optical orientation is a non contact method that creates a spin polarization in a semiconductor by the application of circularly polarized light. It was stated that, for the optical orientation to create any spin polarization, the energy difference between the incident light energy and the bandgap energy should be less than the spin orbit splitting energy ($\hbar\omega - E_g \ll \Delta$). It was explained that the incident light energy for optical orientation in GaAs must be between 1.42 eV (870 nm) and 1.76 eV (705 nm). The degree of electron spin polarization in a zinc-blende semiconductor after optical orientation was stated to be 50%. Holes in a semiconductor can have larger magnetic moments than electrons, and therefore, they are expected to have larger contributions to the optical spin injection.

Spin relaxation, the process by which spin equilibrium is restored was presented. The spin density is expected to decrease exponentially with the inverse time constant $1/T_s = 1/\tau + 1/\tau_s$, where τ_s is the spin relaxation time and τ is the carrier lifetime. The spin relaxation time for heavy-holes was stated to be 110 $\pm$10% fs. In semiconductors, there are four mechanisms by which the carrier spin relaxes: the Elliott-Yafet, D'yakonov-Perel', Bir- Aronov-Pikus,

and hyperfine-interaction mechanisms. The two mechanism that occur in zinc-blende semiconductors, Elliott-Yafet and D'yakonov-Perel' mechanisms were presented with more detail. The Elliott-Yafet mechanism was stated to be the sole origin for the heavy-hole spin relaxation and the dominant one for the light-hole spin relaxation.

Chapter 3

Semiconductors as a source of THz radiation

Terahertz radiation can be produced either by a change in current, or a change in polarization [27]. The strongest THz emission in unbiased semiconductors is generally attributed to two effects: the nonlinear optical rectification effect (polarization change) and the surge photocurrent (current change) produced when a femtosecond optical pulse excites the semiconductor [28]. The THz emissions amplitude depends on several factors such as impurity concentration, excitation wavelength, excitation intensity and externally applied magnetic field [28]. Therefore, by analyzing the THz emissions from a semiconductor, we have a non contact way to study the transient carrier mobility, impurity doping concentration, strength and polarity of the static internal field and even the crystal orientation [29]. In addition to the mechanisms mentioned before, the spin polarization under optical orientation suffers a polarization change, therefore, it is expected to produce a THz radiation as well.

3.1 Optical rectification

Conventional optical rectification occurs when a continuous monochromatic pump beam creates a DC dielectric polarization in the semiconductor, but it does not radiate electromagnetic waves. However, when the semiconductor is optically pumped with an ultrafast pulse train, the different spectral components of the fundamental beam will create a beating polarization. This time varying dielectric polarization produces a transient dipole which radiates electromagnetic waves [30]. Optical rectification is a second order non-linear process produced mainly by two mechanisms, difference-frequency generation and sum-frequency generation [30]. The optical rectification effect is enhanced when high-intensity excitation conditions are used. A characteristic property of this effect is that it depends on the polarization direction of the optical pulse with respect to the crystal orientation of the semiconductor surface [31]. The first model to explain the experimental results from optical orientation was proposed by Schmitt-Rink [32] where it was explained the strong dependence of this effect on crystallographic orientation. It has been experimentally demonstrated [10] that optical rectification in GaAs [33] excited with circularly polarized light do not depend on its handedness. For that matter, the optical rectification contribution to a THz pulse can be discarded by means of lock-in amplification.

3.2 Surge current

To date, it is stated that the surge current of photoexcited carriers can have two origins. One is the built-in electric field proposed by Zhang and Auston [29] where the photoexcited carriers are accelerated by the surface depletion field. The second is the photo-Dember effect, produced by the different diffusion

velocities of the electrons and holes [34, 35].

3.2.1 Built-in static electric field

As a result of Fermi level "pinning" at the interface (Fig. 3.1), both the conduction and valence bands bend causing a different accumulation of charges near the surface of the semiconductor. This mechanism is present in wide-gap semiconductors such as InP and GaAs [29]. The different accumulation of charges produces a static electric field near the surface of the semiconductor. After optical excitation, this electric field will separate photogenerated electrons and holes forming a dipole perpendicular to the surface which emits THz radiation [34]. By changing doping from n type to p type, the sign of the built-in electric field direction is reversed, which changes the polarity of the dipole and therefore changes the sign of the THz transient [34]. This effect does not depend on the incident beam polarization, therefore, its contribution to a THz pulse can also be removed by means of lock-in amplification.

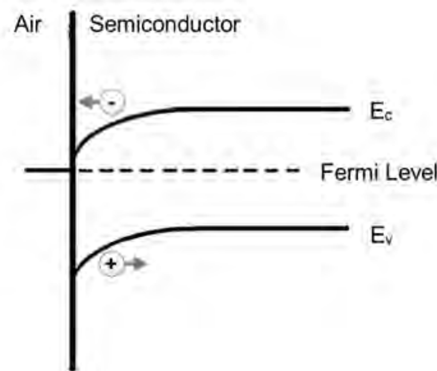

Figure 3.1: Fermi level "pinning" at the interface

3.2.2 Photo-Dember effect

The photo-Dember effect originates from the difference between the diffusion velocities of the electrons and holes [35]. It is produced by two factors: A difference in diffusion coefficients, and a structural asymmetry [34]. Typical semiconductors have larger diffusion coefficients for electrons than for holes, therefore, photoexcited electrons diffuse more rapidly than holes. When this effect occurs near the surface of the material, photocarriers are reflected back and away from the surface creating a dipole perpendicular to the surface. In this case, changing the doping of the material has no effect on the sign of the THz pulse [34]. This effect does not depend on the incident beam polarization and it can be discarded by means of lock-in amplification.

3.3 Injecton and shift currents

Two more photocurrent effects that occur above the bandgap are the injection and shift current. Injection current (circular photogalvanic effect, $\dot{J}(t)$) is proportional to the laser intensity, but it vanishes for cubic crystals. Shift currents [33] (photogalvanic effect, $\dot{P}(t)$) is also proportional to the laser intensity, and it appears in zinc-blende crystals. It is produced by a microscopic shift in the center of charge when the carriers move from the valence to the conduction band [17]. Injection current will vanish in GaAs, due to symmetry in cubic crystals. The shift current will not depend on the polarization handedness of the incident beam, therefore, its contribution to a THz pulse can be removed by means of lock-in amplification.

3.4 Spin polarization and relaxation

The spin polarization of a carrier can be induced when the carrier is photo-generated with circularly polarized light given that it absorbs an amount of angular momentum, as mentioned in Section 1.1. This polarization is expected to emit THz radiation, because flipping a spin will produce a change in magnetic moment [17], and this change of polarization will emit electromagnetic waves similar to the magnetic dipole radiation described in reference [36]. Likewise, the spin relaxation will contribute to the THz pulse with opposite magnitude.

3.4.1 Magnetic dipole radiation

The electromagnetic radiation produced by a magnetic dipole is a well understood process [36]. Using a spherical coordinate system as shown in Fig. 3.2, when a magnetic moment changes along the positive $\mathbf{e_3}$ direction, it will generate an electromagnetic radiation along the $-\mathbf{e}_\phi$ direction, according to equation 3.1

$$(E_{rad})_\phi = -\frac{[\ddot{m}]_{e3}}{c^2 r}\sin\theta \tag{3.1}$$

where m is the magnetic moment, r is the distance from the magnetic dipole center to the observation point, and c is the speed of light. If the radiated electric field is known, and the $\sin\theta$, r and c are fixed, then a double integration over time of the electric field followed by a component rotation of 90° is needed to obtain the magnetic moment. One important fact to consider is that, the positive vertical component $(+\hat{\mathbf{y}})$ of the electric field is produced by a magnetic moment change along $+\hat{\mathbf{x}}$. Similarly, the positive horizontal component $(+\hat{\mathbf{x}})$ of the electric field is produced by a magnetic moment change along -$\hat{\mathbf{y}}$.

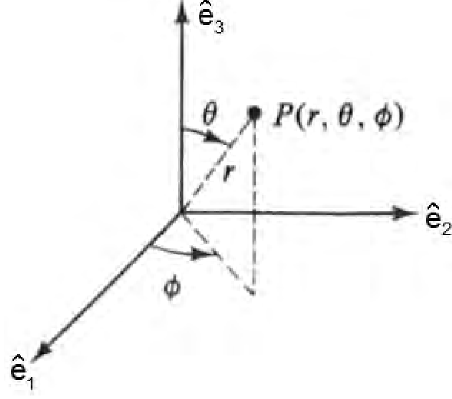

Figure 3.2: Spherical coordinate system

3.4.2 Magnetic moment temporal evolution

In order to understand the temporal evolution of the magnetic moment induced by the photogeneration of spin polarized electron-hole pairs, it can be assumed that the electron-hole magnetic moment magnitude, the carrier density injection rate and the electron-hole spin relaxation are the only mechanisms involved. As mentioned in Section 2.2 , during optical excitation, spin polarized carriers are created and a magnetic moment is formed. For every four photons absorbed, three $m_{e-} = -1/2$ and one $m_{e+} = 1/2$ electrons are created, and consequently, also three ($m_{hh} = 3/2$) heavy-holes and one ($m_{lh} = 1/2$)light-hole appear [17]. It has also been estimated that the ratio of the mean hole magnetic moment to the mean electron magnetic moment ($\bar{\mu_h}/\bar{\mu_e}$) is approximately -27 [17], hence, the hole magnetic moment will have a contribution one order of magnitude larger than electrons.

The carrier density injection rate $\dot{n}$ [17] is described by

$$\dot{n}(\vec{\mathbf{r}}, t) = \xi^{ab}(\omega) E^{a*}_{env}(\vec{\mathbf{r}}, t) E^{b}_{env}(\vec{\mathbf{r}}, t) + c.c. \tag{3.2}$$

where the italic superscripts indicates the Cartesian coordinates that are to be summed over when repeated, $\xi^{ab}(\omega_0)$ is proportional to the absorption coefficient evaluated at a carrier frequency ω, and E^a_{env} is the temporal envelope function of the laser electric field profile $E^a(\vec{\mathbf{r}}, t)$ given by

$$E^a(\vec{\mathbf{r}}, t) = E^a_{env}(\vec{\mathbf{r}}, t) \exp^{-i\omega_0 t} + c.c. \tag{3.3}$$

On equation 3.2, $\xi^{ab}(\omega)$ does not vary much, as shown in [37], over the spectral bandwidth of the laser pulse which is centered at 800 nm with a Full Width Half Maximum (FWHM) of 12 nm. Hence, the temporal behavior of $\dot{n}(\vec{r}, t)$ is only determined by the laser pulse envelope, and the temporal evolution of the magnetization can be modeled using the following parameters: a 50 fs FWHM gaussian beam for optical excitation, a carrier lifetime of 10 ns, a heavy-hole spin relaxation time of 110 fs [16] and a light-hole spin relaxation time of 100 fs [26]. The magnetic moment will increase as the integral of the carrier density injection, and its relaxation will follow the convolution of the carrier density with a decreasing exponential. The temporal evolution of the total magnetic moment (solid line) is presented in Fig. 3.3, as well as the contribution from each carrier. Heavy-holes have the greatest contribution to the magnetic moment generated, both heavy and light holes relax very rapidly ($\sim$ 100 fs), and the electrons magnetic moment contribution remains for a longer period of time ($\sim$ 1 ns) [26]. Once the magnetic moment is obtained, its radiation can be calculated directly. According to equation 3.1, the electric field radiated by a magnetic moment is proportional to its second derivative of its magnitude over time. The magnetic moment (solid line) and the radiated electric field (dashed line) are presented in Fig. 3.4. This simulation was done to have a

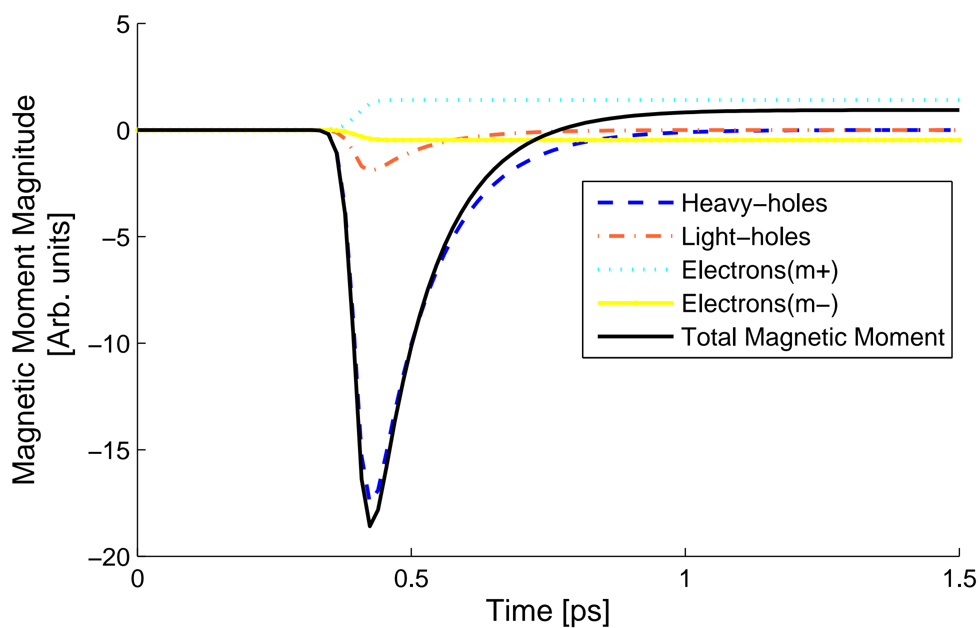

Figure 3.3: Proposed magnetic moment evolution over time and the contribution from all carriers.

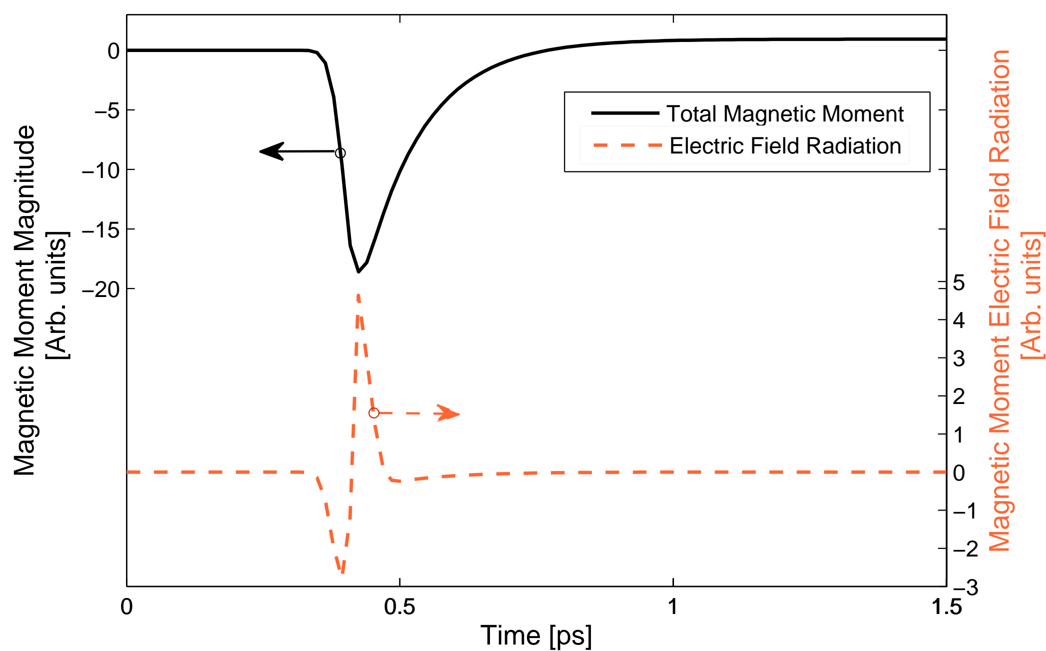

Figure 3.4: Proposed magnetic moment evolution over time and its radiated electric field.

rough idea of the signal expected from the spin polarization and relaxation, however, this is not expected to be a detailed representation of the real process. Many parameters have been ignored such as the whole mechanisms involved during optical orientation and spin relaxation, the limitations by the detector bandwidth, sensitivity and response time, just to mention a few; hence, a more detailed simulation needs to be done to predict the magnetic moment radiation more accurately.

3.5 A brief history of THz in semiconductors

In 1990, Zhang et al. [38] first reported the generation of femtosecond electromagnetic pulses in the THz range from a variety of semiconductors using ultrashort pulses [29]. It was explained that during optical excitation, photons with energy greater than the bandgap are absorbed creating electron-hole pairs that are driven in opposite directions by the built-in static field. This transient current in the depletion layer radiated THz electromagnetic waves [38].This experiment offered a way to generate diffraction-limited electromagnetic beams in the THz range, and also a noncontact, noninvasive way to probe the surfaces of semiconductors [38].

A second experiment was reported by B.B. Hu [39] in collaboration with Zhang, and Auston. In this experiment the semiconductor was optically excited with femtosecond pulses from energies above the bandgap to energies below it. It was shown that, as the exciting energies decreased from slightly above the bandgap, the THz radiation amplitude also decreased and at some point inversed its sign and then increased its amplitude and finally died out.

It means that a THz radiation was induced by the subband-gap femtosecond pulses that do not produce real carriers, and it was proposed that virtual carriers were induced by the short laser pulse and that an electrical transient was induced by a reactive current that was free of the carriers' scattering process [39].

The studies on THz radiation from semiconductors continued and Zhang and coworkers [40] reported a terahertz emission from electro-optic crystals, including semiconductors such as unbiased bulk GaAs. The terahertz emission dependence on azimuthal angle was mapped out when illuminating the (111) and (110) crystal faces of the semiconductor with linearlly polarized light. Some of the semiconductors had bandgap below and above the excitation energy, and comparing the results, it was explained that for photon energies above bandgap both carrier transport and optical rectification can contribute to the radiation, but for energies below bandgap the electromagnetic radiation is only produced by optical rectification since no photocarriers are created [40].

Nastos and Sipe [41] published the most complete theoretical treatment of terahertz response to energies below and above the bandgap in GaAs. It was established that the response above the bandgap is dominated by a shift current, since it is two orders of magnitude larger than the optical rectification and below the bandgap, the response is generated only by optical rectification. Continuing the theoretical work, Sipe and Shkrebtii [42] showed that, when a pulse of light interacts with a semiconductor, the nonlinear polarization induced is

$$P^{(2)}(\Omega) \propto \chi^{(2)} E(\omega) E(\omega - \Omega) \tag{3.4}$$

where the second order susceptibility $\chi^{(2)}$ contains the terms for optical rectification, shift current and injection current [42]. This provided a mathematical expression for some of the mechanisms that generate THz radiation in semiconductors.

A theoretical 3D simulation of the THz generation at semiconductor surfaces was done by Johnston *et.al* [34]. As mentioned before, THz radiation is primarily the result of ultrafast charge transport and optical rectification. In order to study solely the carrier dynamics, this author used a specific crystal orientation and photon energy so that optical rectification is negligible. This way, the analysis was focused on charge transport, specifically surface-field and the photo-Dember effect. The simulation reproduces the processes occurring on the semiconductor before, during and after the photoexcitation, and presents a detailed analysis for GaAs and InAs. Isolating the contribution from each effect on the materials, the simulation shows that InAs is primarily a photo-Dember emitter and GaAs is primarily a surfacefield emitter. The simulation also reproduces the enhancement of the THz emission by the application of a magnetic field which presumably rotates the dielectric dipole allowing more of the dipole radiation to be directed to the surface and then radiated out into free space [34].

A complementary work for this theoretical analysis was carried out experimentally by Ryotaro *et al.* [28] as an attempt to analyze carrier dynamics during photo excitation. Similarly, they used certain crystal orientation to neglect the optical rectification effect and used a lens to focus the optical excitation beam in order to create a small photoexcited region that can be considered as a point source of THz waves from a localized current, in other words, a localized electric dipole moment. The THz emission from the electric dipole is presented

as a function of the incidence angle of the optical excitation. After comparing the results with a mathematical analysis of the dipole, it is concluded that the electric dipole in GaAs is created perpendicular to the surface, but in InAs the electric dipole has a tilt angle to the normal of the surface which is directly related to the incident angle. Furthermore, after applying a magnetic field it is found that the electric dipole in GaAs rotates accordingly with the sign of the magnetic field applied, but the electric dipole in InAs show no significant change in direction. It was mentioned that taking into account a magnetic dipole moment parallel to the surface could explain the effect, but more studies will need to be done to confirm their proposal [28].

Further studies will be performed in order to understand the carrier dynamics that occur during photoexcitation. Meanwhile, in another front, the semiconductors response to circularly polarized light and its subsequent emissions have been studied. Nastos *et al.* [17] first quantified the magnetization injection rate in GaAs, and explored the possibility that the injected magnetization can radiate a detectable terahertz field. The detection of such radiation means a direct observation of the ultrafast magnetization from the optical injection of carriers.

He stated that the ratio of the mean hole-electron magnetic moment ($\bar{\mu_h}/\bar{\mu_e}$) is approximately -27, which means the hole magnetization density is an order of magnitude larger than the electron magnetization and with opposite polarity. To understand the emissions arising from the magnetic injection, he first analyzed the case of a free electron in vacuum. Magnetic dipole radiation from flipping the spin of a free electron in vacuum can be directly compared to the electric-dipole radiation from accelerating an electron through a microscopic dis-

tance [17]. The spin reversal produces a change in magnetic moment $\Delta m = g\mu_B$ and the change in a dielectric dipole is $\Delta p = ea_B$. Comparing these two factors ($\Delta m/\Delta p$) it can be seen that the magnetic radiation is roughly 70 times smaller than the electric-dipole radiation, but it is still above the typical signal-to-noise ratio found in THz measurements [17]. When this calculation is done for excited carriers in GaAs, it is found that the ratio of magnetization to polarization signal is about 0.01 . This calculation already includes effects associated with the temporal behavior of the sources, the transmission of the generated terahertz through the surface, the large magnetic moment associated with the hole, and the actual shift distance associated with absorption [17].

Nastos *et al.* also reported experimentally the terahertz emission from GaAs as a function of the incident light ellipticity at non-normal incidence, and demonstrated that the shift current is maximized when the polarization is linear and minimized when it is circular. On the other hand, the magnetization signal is maximized when the polarization is circular and minimized when it is linear. The ratio between these two signals was 0.017 which is in accordance with the theoretical estimation of 0.01. As a conclusion, it was proposed that the transient during spin carriers formation radiates pulses of electromagnetic radiation in the terahertz range, and it was proposed for future experiments to study the temporal profile of this emitted THz fields and to measure the polarization of the THz as a function of emitted angle [17]. After Nastos experiment, Schmuttenmaer *et al.* [10] reported terahertz emission from GaAs by illuminating at normal incidence, with different ellpticities of the incident beam. The measured data shows a dramatic dependence on the handedness of light when exciting slightly above the bandgap. This dependence was assumed to

be caused by spin polarized electrons modifying the shift currents and causing disagreement between the THz emission and the theoretical predictions. Spin polarized electrons deviate the shift currents, but the reason is not well understood. However, it was confirmed that spin polarized carriers play an important role in the generation of THz radiation.

3.6 Summary

The mechanisms that generate THz in a semiconductor have been presented and discussed. They are: Optical rectification, built-in static electric field, photo-Dember effect, injection and shift current, and spin polarization and relaxation. It was found that all of these effects, except the last one, do not have a dependence on the circular handedness of the incident light or cancel out by crystal symmetry, therefore, the THz contribution of the spin polarization and relaxation can be isolated by means of a lock-in amplifier, which amplifies only the signal changing at certain frequency, in this case, the frequency of the circular polarization modulator. An initial simulation to describe the spin THz emission was proposed. It was also presented a brief history of previous studies on the THz emission from semiconductors that have led to the actual experiment presented in this thesis.

Chapter 4

THz spectroscopy

Some research groups were attempting to generate and detect ultrashort electrical transients as they propagated down a transmission line; the leaders for these groups were: Dan Grischkowsky, David Auston, and Martin Nuss [43]. In 1988-1989 it was first reported the generation of a THz beam which propagated through free space and was detected a few centimeters later [44, 45], and since then, THz emitters and detectors have been developed in order to study materials with THz radiation. This technique is called THz time-domain spectroscopy. A detailed description of a standard THz spectroscopy setup was published by S. R. Keiding *et. al* [46], along with a proposed theoretical model based on the Drude-Lorentz theory. As described in Chapter 3, semiconductors emit THz radiation when excited by ultrashort pulses, hence, analysing their THz emission one can study their carrier dynamics. This technique is called THz emission spectroscopy.

4.1 THz emission spectroscopy

THz emission spectroscopy is specially useful because THz radiation emitted from materials reveal information about their carrier dynamics [4]. A simple THz emission spectroscopy setup is shown in Fig.4.1. During THz emission spectroscopy a sample is photoexcited with visible or near-infrared ultrashort laser pulses, and a current transient and/or a polarization transient at the sample generates a detectable THz emission [27]. The THz radiation emitted is very sensitive to carrier density and mobility, so terahertz systems are used to obtain information about the material properties. THz emission spectroscopy has already been used to study carrier dynamics in GaAs [47, 48], InP [49, 50], InN [51] and semiconductor polymers [52], just to mention a few.

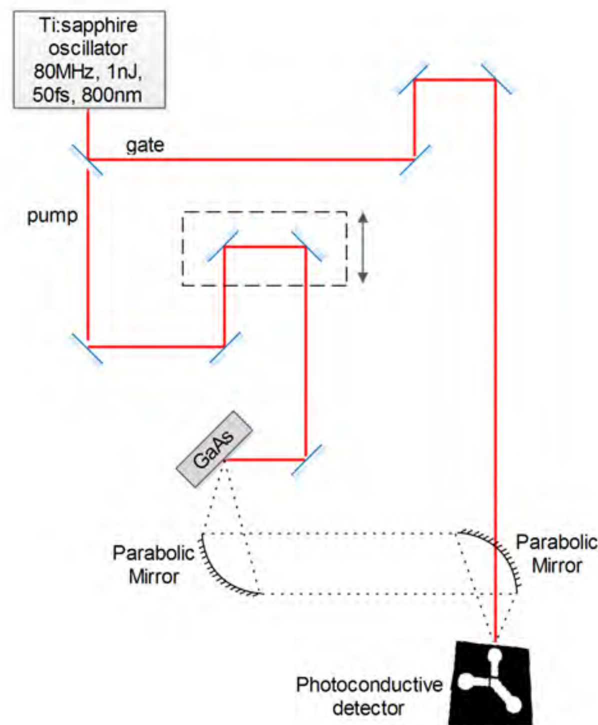

Figure 4.1: THz emission specctroscopy setup

4.2 THz detection

The techniques used to detect radiation are based on two main effects: the first is the radiation ability to heat a body in which it is absorbed, and devices based on this effect are called thermal detectors; the second effect is due to the interaction of radiation with single electrons when the energy of a photon is given to an electron to free it from a bound state, detectors based on this effect are called photoelectric detectors [53]. Thermal detectors used to detect THz radiation such as the thermopile [54], the bolometer [55] or the Golay cell [56] need a controlled environment which requires cooling systems and are not fast nor sensitive enough to deliver a precise detection of the THz emission. Photoelectric devices such as the Schottky diodes are used over the whole infrared spectrum in a number of laboratories and are superior than thermal devices on specific purposes [53]. Two commonly used THz detection methods, based on photoelectric devices, are: Free space electro-optic sampling, and the photoconductive detection.

4.2.1 Free space electro-optic sampling

Free Space Electro-Optic Sampling (FSEOS) is based on the Pockels effect, where an applied voltage causes birefringence in a crystal. When an optical sampling pulse travels through a crystal at the same time as the THz pulse, its polarization is slightly rotated due to the THz electric field. The magnitude of the rotation is proportional to the magnitude of the THz field, and the direction of rotation is proportional to the sign of the field. The detector crystal is usually a 0.5-1.0 mm thick (110) ZnTe crystal which exhibits a similar refractive index for the infrared and THz bands that permits a velocity matching for the beams

propagation inside the crystal [27]. A quarter-wave plate, a Wollaston prism and a pair of balanced diodes are used in that order after the detector crystal to measure the sampling pulse rotation. A lock-in amplifier phase-locked to an optical chopper collects the signal from the diodes which is proportional to the THz electric field. The complete THz pulse is then mapped out as a function of time by moving the arrival time of the optical sampling pulse with respect to the THz signal. The THz system is usually enclosed and purged with dry nitrogen to minimize THz absorption by water vapor [27].

FSEOS is the preferred technique when an amplified laser system is used. It offers a flat frequency response over a wide bandwidth, it is purely optical, so it does not need electrode contacts or wirings, it is a non-resonant method of detection, so there is a low risk for damaging the detector crystal with the focused beam [57]. One disadvantage of FSEOS is that it can only record one polarization component at a time. In order to record more than one polarization of the THz signal, it would be required to rotate the polarization of the beams or optical devices which may produce misalignments that will cause a shift in the phase of the electric field components, and the data acquisition time is increased due to the realignment of the components after each measurement [58]. Paul Planken [59] has proposed a modified FSEOS setup which offers the possibility of simultaneously measure both transversal electric field components. It uses an extra half-wave plate and changes the ZnTe crystal orientation to (111), which reduces the signal to 18% compared to the commonly used (110) orientation, hence, this proposed method is not optimal for small signal detection.

4.2.1.1 Polarization resolution limitations of FSEOS with (110) ZnTe

As mentioned in section 3.5, it has been presented by Nastos [17] a preliminary measurement of the spin transients THz radiation detected by FSEOS. The detected signal in a ZnTe crystal directly depends on the angle (α) between the THz electric field and the probe beam electric field at the (110) crystal face. According to measurements in the literature [60], the magnitude of the detected signal when the angle α is 0° and 90° is basically the same, with a reversed sign. FSEOS detection uses a Lock-in Amplifier which measures the total amount of change in the signal, its phase is adjusted in order to maximize the signal, hence, (110) ZnTe FSEOS detection can not resolve between a horizontally or vertically polarized THz electric field.

4.2.2 Photoconductive detection

A photoconductive detector is made of a pair of metallic contacts deposited on a semiconductor substrate. An ultrashort laser pulse (gate beam) synchronized with the THz beam are focused on the gap between the two contacts. The laser pulse photoexcites the semiconductor creating photocarriers that will be accelerated under the THz electric field producing a measurable current between the contacts [61]. One consideration for these detectors is that the production of ultrashort currents, and therefore the performance of the photoconductive detector, strongly depends on the carrier trapping and recombination lifetimes of the semiconductor where the device is fabricated [62]. There are two operational modes for photoconductive detectors depending on their carrier lifetimes: direct sampling detectors and integrating detectors.

Direct sampling detectors are usually made of highly resistive semiconductor substrates with short charge-carrier lifetimes. The carrier lifetimes are shorter or comparable to the laser pulse, hence the detector will sample only the point of the THz signal that overlaps temporally with the laser pulse. The detected photocurrent will be related to the THz electric field (E_{THz}) as

$$I(t) \propto E_{\mathrm{THz}}(t) \tag{4.1}$$

Integrating detectors are commonly fabricated from materials with carrier lifetimes longer than the duration of the THz signal. The photoconductive detector will record all the current generated by the THz transient after optically excited by the laser pulse. The measured current will be proportional to the integral of E_{THz}

$$I(\tau) \propto \int_{\tau}^{\infty} E_{\mathrm{THz}}(t)dt \tag{4.2}$$

where τ is the arrival time of the laser pulse with respecto to the THz signal [63].

Photoconductive detectors have proven to be useful for THz detection, however, the necessity to analyze terahertz pulses with more detail has lead the research for polarization sensitive detectors. A new kind of photoconductive detectors can measure two of the electric field components at the same time. Three different detector designs have been presented by Hussain [64], Makabe [65] and Castro-Camus [62] independently; and they simplify the polarization pulse acquisition by measuring the entire wave simultaneously [58].

A diagram of the multicontact photoconductive detector designed by Castro-Camus is shown in Fig. 4.2. There are two main constrains for these multi-contact detectors: first, the gap between the ground contact and the other two

Figure 4.2: Three contact photoconductive detector designed by Castro-Camus

contacts need to be orthogonal, and second, both gaps must be within an area smaller than the laser beam waist and the focus spot size of the THz radiation (a circle of radius $\sim 100\,\mu m$) in order to have uniform laser and THz illumination across both gaps [62]. The photoconductive detector specifically used for this work was made on a substrate of (Semi-Insulating) SI-GaAs followed by a layer of SI-GaAs (200 nm), a layer of AlAs (100 nm), a layer of implanted As+ ions into SI-GaAs (1200 nm) to a fluency of $1.0 \times 10^{13}\,\mathrm{cm}^{-2}$ at 2.4 MeV and $2.5 \times 10^{12}\,\mathrm{cm}^{-2}$ at 1 MeV. It has carrier lifetimes larger than 100 ps, therefore it falls into the integrating detectors category described before; the three conductive contacts were made of a gold layer (250 nm) over a thin layer of chromium (20 nm); and the gaps width was 16 μm with the edges extended over 100 μm [61].

A characterization of the signal-to-noise, spectral response and polarization resolution of a similar photoconductive detector has already been done [66]. It was found that Johnson-Nyquist and laser shot noise are the two main sources of noise; basically white noise because they have no dependence on frequency. The signal to noise ratio is almost constant as a function of frequency except for very low frequencies (< 10 Hz). The dynamic range of the detector is around two

orders of magnitude (40 dB) under optimal operation conditions. The usable bandwidth of the detector was found to be ~ 4 THz (from ~ 50 GHz to approximately 4 THz before the signal reaches the noise floor) and the polarization angular resolution $\sim 0.34°$ [66]. This three contact photoconductive detector has been extensively characterized and has shown to be an accurate device to measure two orthogonal polarization components of THz radiation [61].

4.2.2.1 Photoconductive detector alignment

For an optimal performance of the photoconductive detector, the gate laser beam and the THz beam should be aligned at the center of the three contacts [61]. To achieve this, the following steps should be followed.

- Block the gate beam.
- Replace the THz emitter by a diffusor (e.g. tracing or Bond paper) to generate a visible spherical wavefront that will follow the same path through the parabolic mirrors as the THz would do.
- The focus of the visible wavefront after the second parabolic mirror should hit one of the gaps. This can be done by measuring the resistance at one gap and adjusting the detector position until the resistance is minimized.
- The X, Y and Z position of the detector is adjusted to minimize the resistance at the same gap, in order to align the center of the gap and the focus of the parabolic mirror.
- Block the THz beam and unblock the gate beam.
- Without moving the detector, adjust the gate beam position to minimize the resistance in the same gap. This will align the center of the gap, the

gate beam and the focus of the parabolic mirror.

- Finally, adjust the detector position to minimize equally the resistance in both gaps.

More detailed instructions can be found in references [61] and [66].

4.3 Summary

THz emission spectroscopy was presented as a useful tool to analyze temporally evolving processes, such as carrier dynamics. Two of the main detection techniques, free space electro-optic sampling and photoconductive detection, have been presented. A recently developed polarization-resolved photoconductive detector has been described. The signal measured by such detector was stated to be a time integral of the THz electric field. Its usable bandwidth was stated to be $\sim 4\,\mathrm{THz}$

Chapter 5

THz emission spectroscopy of bulk GaAs

5.1 Experimental setup

The optical arrangement used to investigate the THz emission from the bulk GaAs sample is presented in Fig. 5.1. From top to bottom, a Ti:sapphire oscillator delivers 33 fs pulses at a repetition frequency of 80 MHz, centered at 800 nm, with a total power of 270 mW. The laser beam from the oscillator is linearly p-polarized. The beam is split into a pump beam with nearly all the power $\sim 90\%$ and a gate beam with the rest of the power, which is used as an optical gate at the detector. The pump beam goes through an optical chopper locked to 390 Hz necessary for lock-in detection. The pump beam polarization is controlled by a liquid crystal retarder (LCR) and an achromatic quarter-wave plate (QWP). The LCR acts as a half-wave plate whose fast axis is oriented at 45° from the $\hat{\mathbf{x}}$ axis (see Fig.5.1). Modulation of the LCR rotates the beam polarization by 90° , switching the beam polarization from (p) horizontal to (s)

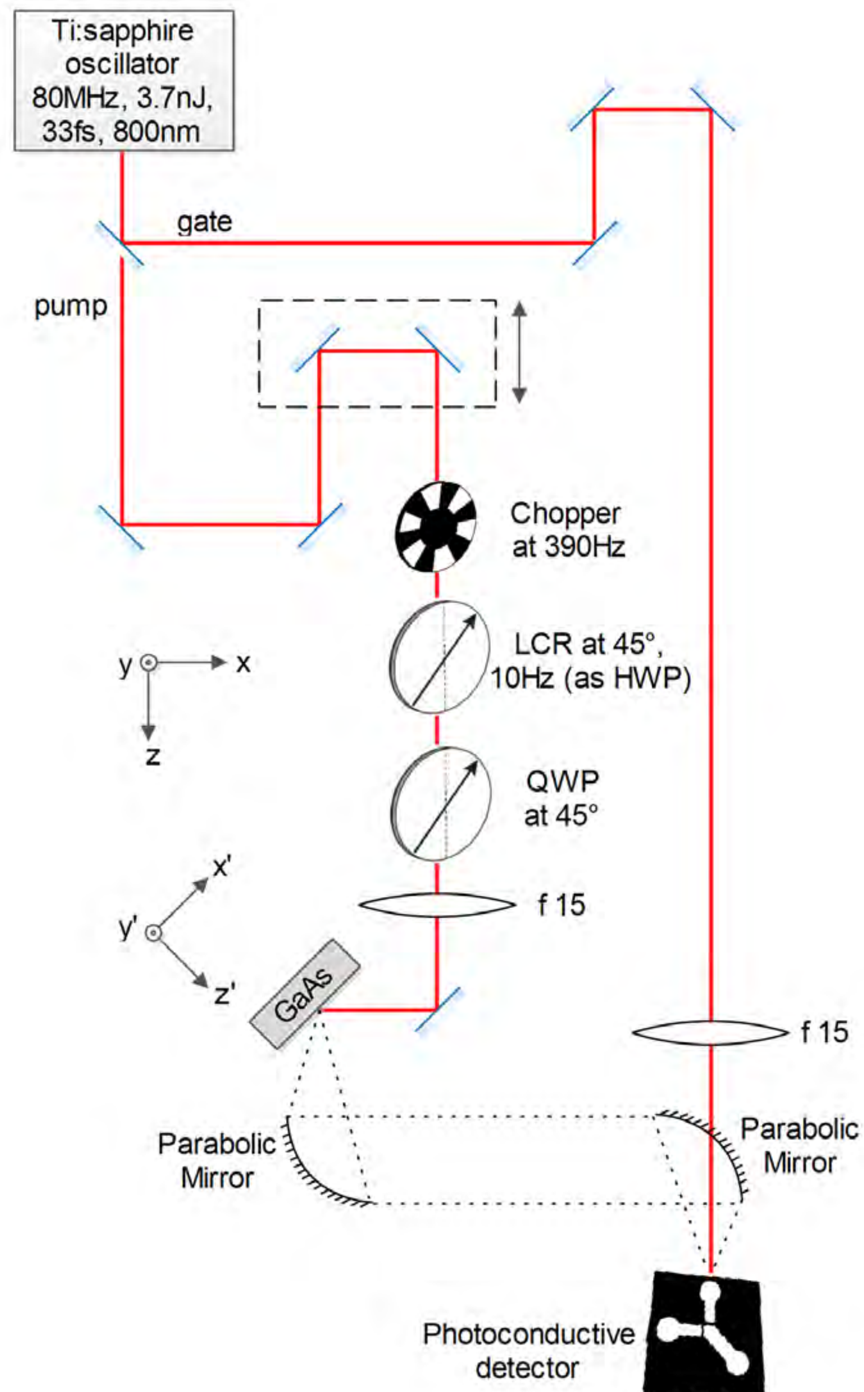

Figure 5.1: Experimental Setup

vertical at a frequency of 10 Hz. The QWP is also oriented at 45° from the $\hat{\mathbf{x}}$ axis, so it generates right and left circularly polarized light. The pump beam is then focused by an optical lens (focal length, 15 mm) to reduce the excitation area at the GaAs surface, however, the sample is not placed exactly at the laser beam focus in order to produce a more collimated THz emission. The pump beam illuminates the GaAs (100) face at an incidence angle of 45° with respect to the surface normal ($\hat{\mathbf{z}}$**'**) as shown in Fig.5.1, the pump is refracted inside the sample to an angle of $\sim$ 11°. The emitted THz radiation is collected at 45° by an off-axis parabolic mirror, whose focal point is aligned to coincide with the emission source point of the sample. The first parabolic mirror collimates the THz radiation which is then focused again, with a mirror of the same type, into the photoconductive detector described in section 4.2.2. Simultaneously, an optical lens (f=15 mm) is used to focus the gate beam onto the photoconductive detector. The focus point of the pump and gate beams must spatially coincide with the central area between the three contacts of the detector. Alignment instructions can be found in section 4.2.2.1. In this experiment, the detector position was optimized and the resistance at the gaps (when illuminated by the gate beam only) was minimized to 19.9 MΩ for both of them. The signals from the photoconductive detector goes into lock-in amplifiers phase-locked to the optical chopper at a frequency of 390 Hz to obtain the complete THz pulse signal, which is then filtered again by a second pair of lock-in amplifiers phase-locked to the LCR frequency to obtain the signal contribution oscillating at 10 Hz. The experiment was performed at room temperature. All devices from the sample to the detector were enclosed in a vacuum chamber and purged with dry nitrogen to replace air and minimize THz absorption by water vapor.

5.2 THz radiation from optically excited bulk GaAs

Ultrashort laser pulses produce several effects in semiconductors, as mentioned in Chapter 3, such as optical rectification, surface field emission, photo-Dember emission and in addition to those, if present, a magnetic moment transient that will also have a small contribution to the THz emission. Using the experimental setup shown in Fig. 5.1, a SI-GaAs sample was optically excited with circularly polarized light. The signal measured by the photoconductive detector was processed by a lock-in amplifier configured with a time constant of 300 ms, a sensitivity of 100 μV, and referenced to a square signal of 390 Hz (mechanical chopper frequency). This lock-in amplifier delivers the complete THz radiation signal including all the effects mentioned in Chapter 3. The two orthogonal polarization components of this signal are shown in Fig. 5.2 as a solid line; the top plot shows the vertical ($\hat{\mathbf{y}}$) component, and the bottom plot shows the horizontal ($\hat{\mathbf{x}}$) component. Twenty measurements were averaged to obtain this signal.

In order to obtain the THz emission which depends on the handedness of the circularly polarized light, the first lock-in time constant was reconfigured to 10 ms, and its amplified output was used as input for a second lock-in amplifier. The output of the first lock-in has an amplification of 10 V per sensitivity step, hence the amplification can be calculated as 10 V/100 μV=100,000. The second lock-in was configured with a time constant of 1 s, a sensitivity of 20 mV, and referenced to a square signal of 10 Hz (LCR working frequency). The second lock-in amplifies only the signal which is circular-polarization dependent by 500 times (10 V/20 mV=500). This lock-in measures the signal difference

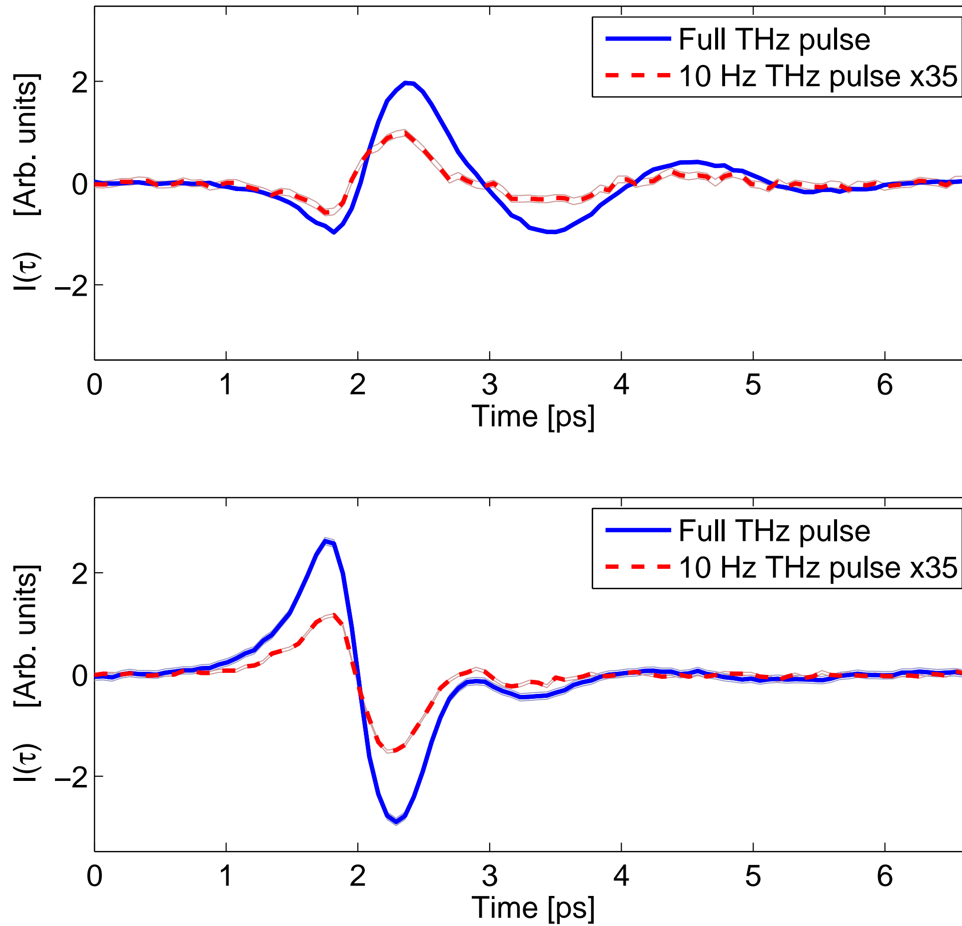

Figure 5.2: Polarization components of the signal at the photoconductive detector $I(\tau)$. Top graph shows the vertical ($\hat{\mathbf{y}}$) component. Bottom graph shows the horizontal ($\hat{\mathbf{x}}$) component. The solid line is the complete THz pulse from the bulk GaAs, including optical rectification, photo-Dember effect, surface field emission and spin transient emission. The dashed line is only the contribution which is oscillating at 10 Hz (LCR frequency); it is multiplied by 35 for visual clarity.

between the two polarization states (left and right circular polarization) which have same magnitude but opposite sign, hence the output signal would be two times bigger and it must be divided by half to reflect the real magnitude. Once the amplifications have been taken into account, the signals from both lock-ins can be compared and it is found that the signal from the THz pulse (first lock-in) is around ~ 70 times larger than the signal oscillating at 10 Hz (second lock-in), which means a ratio of 0.014. The two orthogonal components of the 10 Hz signal are presented in Fig. 5.2 as a dashed line. One hundred and twenty measurements were averaged to obtain this signal. It has been multiplied by 35 for visual clarity.

As mentioned in section 4.2.2, the photoconductive detector delivers a signal which is the time integral of the THz electric field, hence, the signal obtained from the detector has to be differentiated over time to obtain the THz electric field. Fig. 5.3 presents the two electric field polarization components, their 3D combination and their evolution over time. The vertical and horizontal components of the detected electric field are plotted at the vertical and horizontal axes respectively. At the center of the figure, with a lighter line, a 3D representation of the total electric field is shown. It can be noticed that the electric field is basically oscillating over one single plane which means most of the signal is linearly polarized. But the THz emission from the sample was expected to be mainly along the horizontal plane, because a polarization transient along $\hat{\mathbf{x}}$ will radiate a THz field along $\hat{\mathbf{x}}$ (most of the THz emission sources are in this category). However, the signal polarization plane is rotated $\sim 20°$ from the horizontal plane, which could be explained by a slight rotation found at the detector with respect of its supporting base (see inset in Fig. 5.3). A computational rotation of the signal was done to compensate for this misalignment

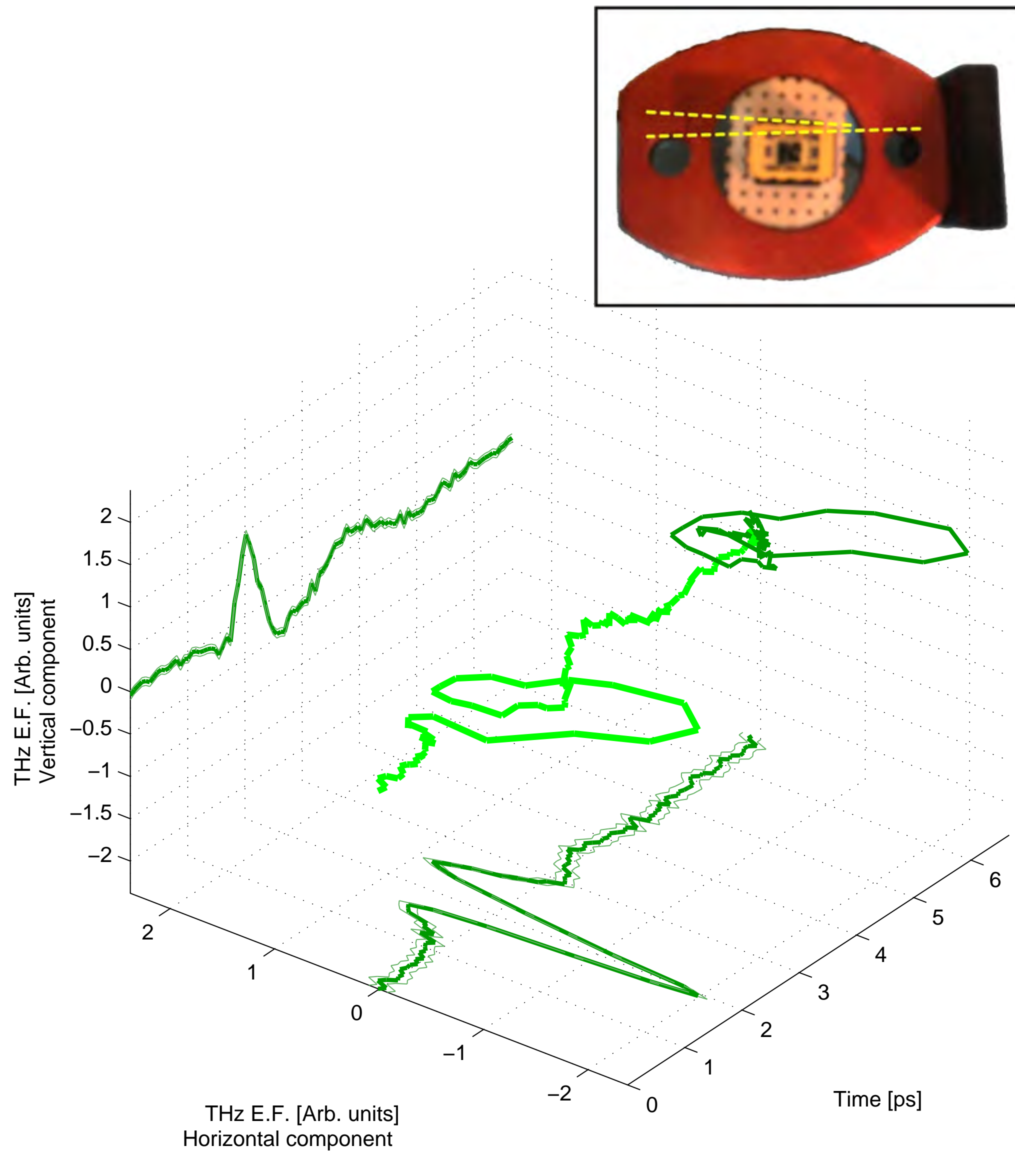

Figure 5.3: Polarization components of the THz electric field at the detector and their evolution over time.

in order to show a more accurate representation of the carrier dynamics in the sample. Once the THz electric field is rotated, the transmission coefficients for p-polarized and s-polarized electric fields are considered at the sample surface. Bulk GaAs shows a refractive index of ~ 3.69 at the THz regime, and the electric field detected at 45° should come from a beam propagating at 11° inside the sample. The set of equations to calculate the transmission coefficients of a material [9] are:

$$t_s = \frac{2\sin\theta_t\cos\theta_i}{\sin(\theta_i+\theta_t)}, \qquad t_p = \frac{2\sin\theta_t\cos\theta_i}{\sin(\theta_i+\theta_t)\cos(\theta_i-\theta_t)} \tag{5.1}$$

and the transmittance for each polarization component is

$$T_s = \frac{n_t\cos\theta_t}{n_i\cos\theta_i}t_s^2, \qquad T_p = \frac{n_t\cos\theta_t}{n_i\cos\theta_i}t_p^2 \tag{5.2}$$

where n is the refractive index, the angle θ with subindex i means *angle of incidence*, and with subindex t means *angle of transmission*. Hence, the calculated transmittances are $T_p = 0.79$ and $T_s = 0.55$. Dividing the electric field components by its proper transmission coefficient (Horizontal/T_p, Vertical/T_s) will reveal the complete THz electric field inside the sample, which is presented in Fig. 5.4. Similarly, the signal contribution oscillating at 10 Hz is differentiated over time, rotated by the same degree and divided by the proper transmission coefficients. The resultant signal is presented in Fig. 5.5. Additionally, a set of measurements were taken with the optical axis of the LCR and QWP at 0°, and the signal oscillating at 10 Hz disappeared confirming that it comes from the QWP and the LCR. The complete THz pulse did not show any change, confirming that the plane rotation was caused by the detector and not by a secondary effect of the spin polarization.

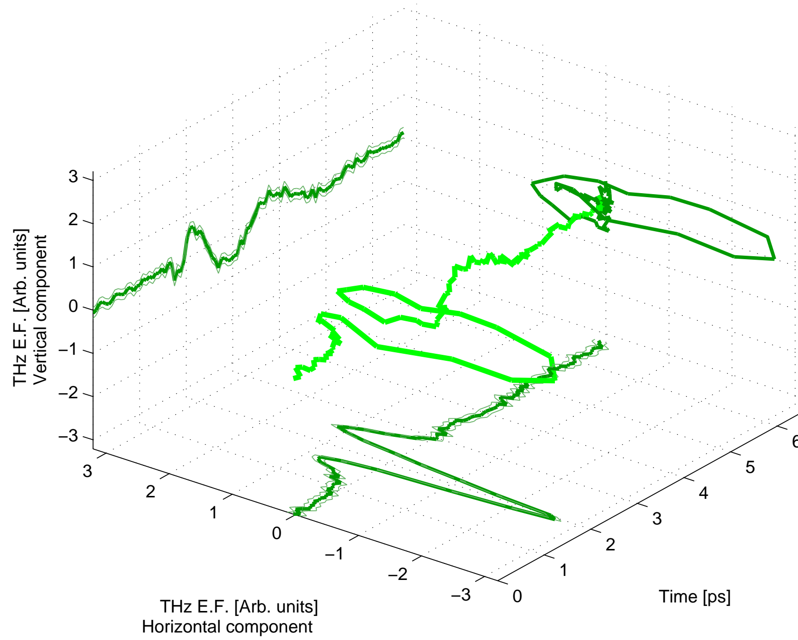

Figure 5.4: Polarization components of the THz electric field inside the sample and their evolution over time.

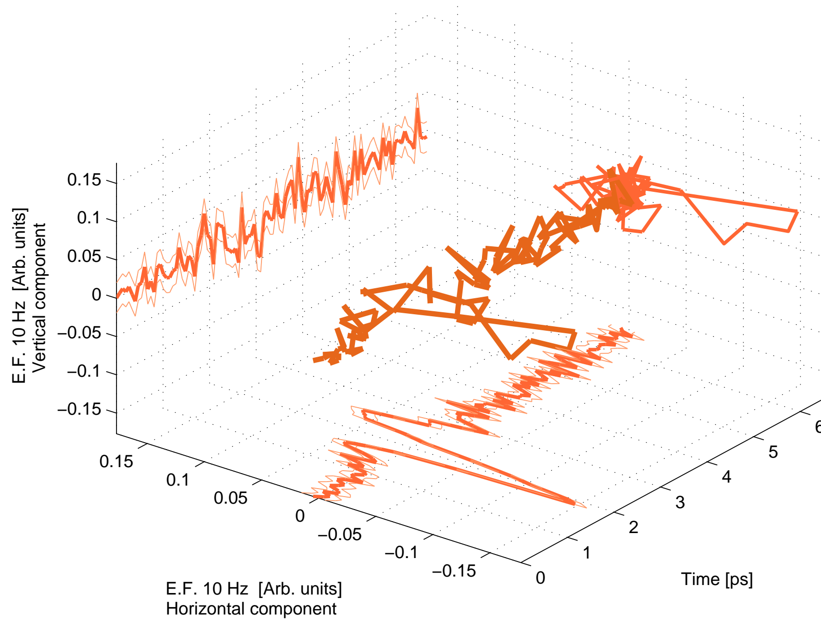

Figure 5.5: Polarization components of the 10 Hz THz electric field inside the sample and their evolution over time.

5.3 Signal analysis

The THz electric field at 10 Hz is assumed to be only emitted by a magnetic source (spin polarization/relaxation). As described in section 3.4.1, a magnetization source along $\hat{\mathbf{x}}$ will radiate a THz electric field along $\hat{\mathbf{y}}$. However, the signal oscillating at this frequency lay along ($\hat{\mathbf{x}}$). It can be noticed from Figs. 5.4 and 5.5 that the complete THz signal and the one oscillating at 10 Hz have a very similar shape, which suggests that it might be produced by some other effect and not only the spin polarization. It was found that the LCR does not transmit the same amount of power when it acts as a half-wave plate and when it acts as an isotropic glass. A power meter was used to measure the beam power that the LCR transmits on its own, and it was found a difference of ~ 1 mW. The same measurement was performed at the sample position, with all the optical arrangement in place, and a difference of ~ 0.5 mW was found. This power difference is oscillating at 10 Hz in synchrony with the LCR, and it explains why the signal in Fig. 5.5 is very similar to the complete THz pulse shown in Fig. 5.4.

In order to balance the transmitted energy from the LCR, a tilted microscope slide was used as a beam splitter just after the LCR to reflect part of the p-polarized beam in order to balance the transmitted energy for the two LCR states. The angle of the microscope slide was adjusted to $12°$ with the help of a photodiode and a lock-in amplifier in order to minimize the energy difference. This part of the optical arrangement is shown in Fig. 5.6.

When the energy transmitted by the LCR was balanced, a new set of measurements were taken. In the new measurements, it was still found a

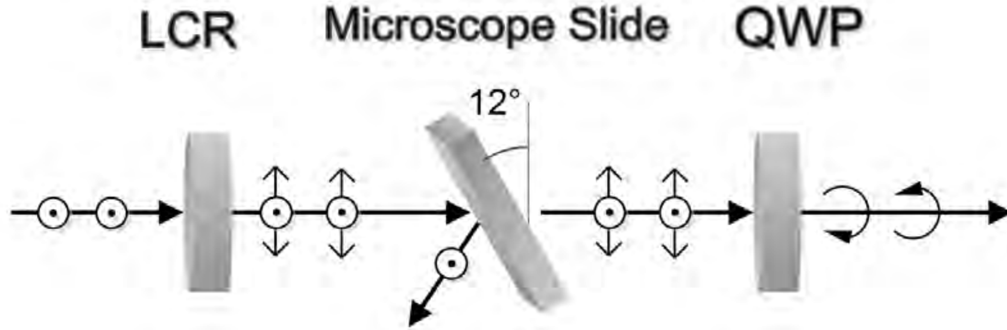

Figure 5.6: A microscope slide is used to balance the energy transmitted by the two LCR states

small replica of the complete THz pulse on the horizontal plane, but now it is ∼ 250 times smaller than the complete THz pulse (which is mainly surface field emission), as shown in Fig. 5.7. This new measurements present a ratio of ∼ 0.004 between the complete THz pulse and the one oscillating at 10 Hz. However, there is still no signal in the vertical polarization where the spin THz emission is expected. Similarly to the previous measurements, the signals were rotated to adjust the detector misalignment, compensated for the Fresnel coefficients, and differentiated over time to obtain the electric field. The THz electric field of the complete emitted pulse is shown in Fig. 5.8, and the THz electric field oscillating at 10 Hz is shown in Fig. 5.9.

According to Nastos *et al.* [17] the ratio between the shift current THz emission and the spin THz emission was found theoretically to be ∼ 0.01; and an initial experiment was presented using a Ti:sapphire oscillator where they found the presence of a signal with a ratio of ∼ 0.017 . In a similar optical arrangement but using a parametric amplifier, van Driel [33] estimated the radiated THz electric field from the shift current in GaAs to be ∼ 2 V/cm. On the other hand, GaAs is primarily a suface field emitter [34], and it has been estimated

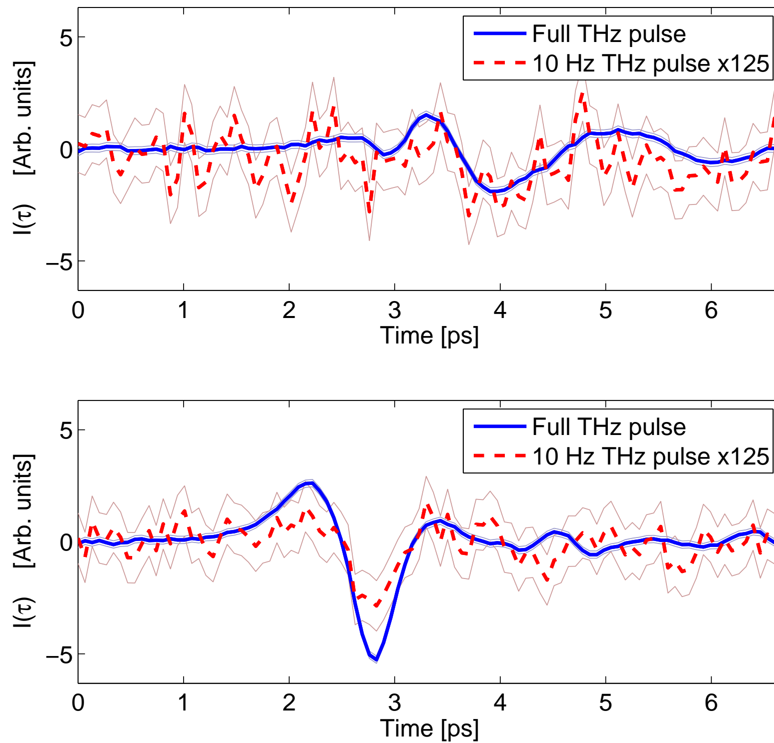

Figure 5.7: Polarization components of the signal at the photoconductive detector $I(\tau)$ after the LCR was balanced. Top graph shows the vertical ($\hat{\mathbf{y}}$) component. Bottom graph shows the horizontal ($\hat{\mathbf{x}}$) component. The solid line is the complete THz pulse. The dashed line is only the contribution which is oscillating at 10 Hz (LCR frequency); it is multiplied by 125 for visual clarity.

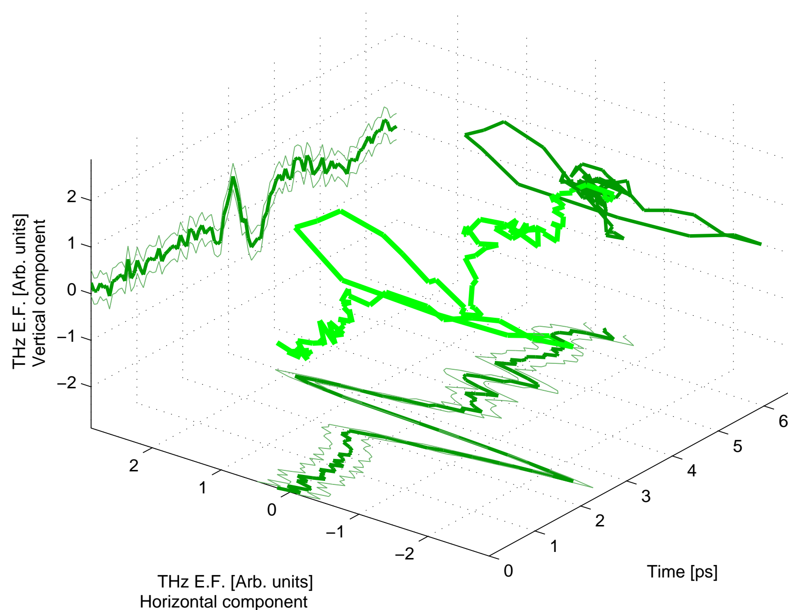

Figure 5.8: Complete THz pulse electric field after power balanced with microscope slide.

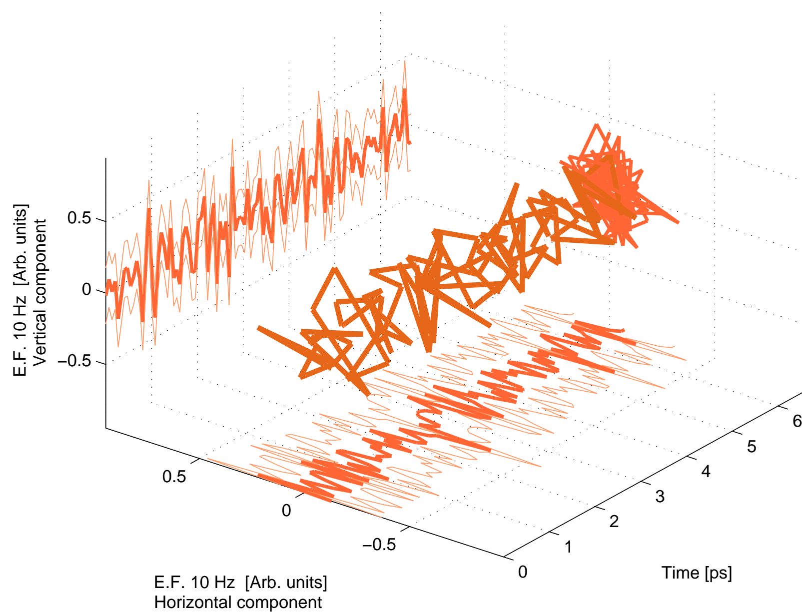

Figure 5.9: THz electric field at 10 Hz after power balanced with microscope slide.

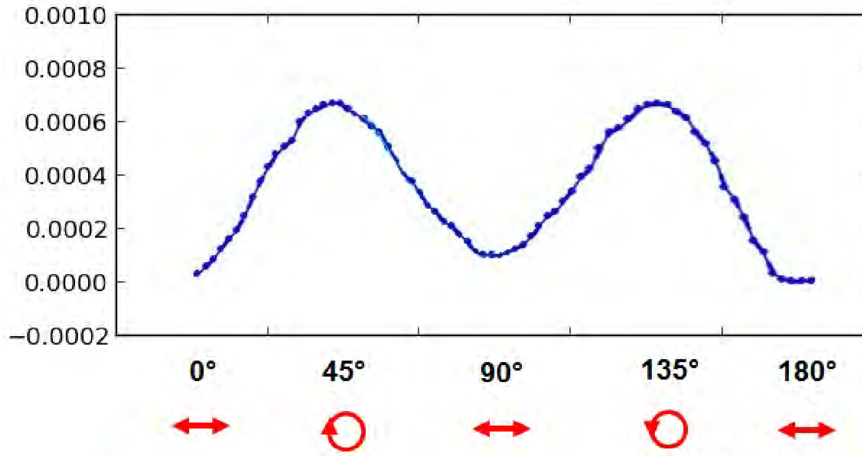

Figure 5.10: Angular dependency of the LCR output power.

by Auston *et al.* [39] that the amplitude of the THz radiation produced by the surface field effect in GaAs would be about a few V/cm. Hence, the normal emitted electric field from the shift current in Nastos experiment and the electric field radiated by the surface field effect in this thesis experiment are around the same order of magnitude. However, in this experiment, a signal ~ 250 times smaller than the surface field emission was detected, but the spin emission which is supposed to be around a ~ 100 times smaller was not found. Therefore, the result of this experiment opens the possibility that the THz radiation emitted by spin transients might be smaller than the theoretical proposal, and it might be the reason why it was not detected in the present experiment.

Furthermore, the angular dependency of the LCR output power was measured, and the power difference between the two states for different angles of the LCR optic axis is shown in Fig. 5.10. This curve has a similar shape as the one measured by Nastos *et al.* (Ref. [17], Fig. 4b). Hence, the possibility that this previous experiment detected a signal from a small modulation of the pump power and not from the spin transients is suggested.

Additionally an effort to estimate the magnitude of the optical susceptibility pseudotensor λ^{abc} is presented here. In Ref. [17] it is stated that the microscopic expresion for the magnetization-injection rate is

$$\dot{\mathbf{M}}^{a}_{inj}(\vec{\mathbf{r}},t) = \lambda^{abc}(\omega)E^{b*}_{\mathrm{env}}(\vec{\mathbf{r}},t)E^{c}_{\mathrm{env}}(\vec{\mathbf{r}},t) + c.c. \tag{5.3}$$

and in a similar form, the polarization-injection rate is described by

$$\dot{\mathbf{P}}^{a}_{inj}(\vec{\mathbf{r}},t) = \sigma^{abc}(\omega)E^{b*}_{\mathrm{env}}(\vec{\mathbf{r}},t)E^{c}_{\mathrm{env}}(\vec{\mathbf{r}},t) + c.c. \tag{5.4}$$

where σ^{abc} is a third-rank susceptibility tensor.

The magnetization-injection rate has been shown to be at least 250 times smaller than the polarization-injection rate, hence, it can be assumed that the relation $250\,\dot{\mathbf{M}}^{a}_{inj}(\vec{\mathbf{r}},t) < \dot{\mathbf{P}}^{a}_{inj}(\vec{\mathbf{r}},t)$ is true, and consequently the relation $\lambda^{abc} < \sigma^{abc}/250$ should also be true. Sipe [42] presented the values for the susceptibility tensor σ^{abc}, where it is found to be $\sim 1\times10^{5}\mathrm{A/V^2}$. Therefore, it is estimated that λ^{abc} should be less than $4\times10^{2}\mathrm{J/V^2m}$.

5.4 Summary

The experimental setup used to search the spin THz emission was explained. The THz emission spectroscopy was used to measure the emission of GaAs. The measured signals were presented and processed for a better study. A signal analysis discovered an energy difference at the pump beam produced by the LCR. A beam splitter was used to correct it. A new set of measurements showed that a horizontally polarized signal ~ 250 times smaller than the complete pulse

could be detected, however, the spin THz signal, expected to be ~ 100 times smaller, was not found.

Chapter 6

Conclusions

This thesis presents the investigation of THz radiation emitted when carriers are optically excited with circularly polarized light; since the optical orientation transient and the spin relaxation transient are expected to emit a THz radiation. We observed a small signal that was related to the handedness modulation with a magnitude comparable to previously reported experiments but with a polarization in the wrong direction, after performing a careful analysis we found that this signal was caused by a modulation of power produced by the pump polarization modulator. After compensation for this power modulation no signal could be observed. The result of this experiment suggests the possibility that the previous reports (which do not have THz polarization resolution) could have measured a power modulation unrelated to the spin dynamics.

6.1 Further work

In this work it was presented an investigation of THz radiation emitted from spin polarization/relaxation of photogenerated electron-hole pairs. A simple model to predict the temporal evolution of the magnetization was presented, yet, it can be improved to describe the temporal profile with more detail if all the parameters involved are taken into consideration. On the experimental side, an unexpected power modulation at the pump polarization modulator produced a small THz signal polarized in the wrong direction, which can be avoided in further experiments using a polarization modulator which delivers the same amount of power for both states when it is switching. Removing this unexpected signal will permit the detection of the THz radiation which is dependent on the handedness polarization only. The THz spectroscopy system can also be improved to detect smaller THz signals by developing a more sensitive multi-contact photoconductive detector. This can be achieved by using a different substrate material sacrificing the recombination lifetimes but increasing the carrier trapping which is translated into higher sensitivity at the THz detection.

Bibliography

[1] A. Markelz, S. Whitmire, J. Hillebrecht, and R. Birge. *Thz time domain spectroscopy of biomolecular conformational modes*. Phys. Med. Biol., 47:3797, 2002. 1

[2] B. Ferguson and X.C. Zhang. *Materials for terahertz science and technology*. Nature Materials, 1:26, 2002. 1

[3] L. Ozyuzer, A. E. Koshelev, C. Kurter, N. Gopalsami, Q. Li, M. Tachiki, K. Kadowaki, T. Yamamoto, H. Minami, H. Yamaguchi, T. Tachiki, K. E. Gray, W.-K. Kwok, and U. Welp2. *Emission of coherent thz radiation from superconductors*. Science, 318:1291, 2007. 1

[4] Ronald Ulbricht, Euan Hendry, Jie Shan, Tony F. Heinz, and Mischa Bonn. *Carrier dynamics in semiconductors studied with time-resolved terahertz spectroscopy*. Rev. Mod. Phys., 83:543, 2011. 1, 38

[5] Gordon Moore. *Cramming more components onto integrated circuits*. Electronics Magazine, 38:8, 1965. 2

[6] Gary A. Prinz. *Magnetoelectronics*. Science, 282:1660, 1998. 2

[7] I. Žutić, J. Fabian, and S. D. Sarma. *Spintronics: Fundamentals and applications*. Rev. Mod. Phys., 76:323, 2004. 2, 4, 5, 7, 8, 9, 12, 13, 14, 15, 17

[8] F. Meier and B. P. Zakharchenya. *Eds. Optical Orientation*. North-Holland, New York, 1984. 3

[9] Eugene Hecht. *Optics*. Addison Wesley, 1987. 3, 54

[10] James M. Schleicher, Shayne M. Harrel, and Charles A. Schmuttenmaer. *Effect of spin-polarized electrons on terahertz emission from photoexcited gaas*. J. Appl. Phys., 105:113116, 2009. 4, 24, 35

[11] Y. Ohno, D. K. Young, B. Beschoten, F. Matsukura, H. Ohno, and D. D. Awschalom. *Electric spin injection in a ferromagnetic semiconductor heterostructure*. Nature, 402:790, 1999. 8

[12] Alexander Khaetskii. *Nonexistence of intrinsic spin currents.* Phys. Rev. Lett., 96:056602, 2006. 8

[13] N. F. Mott. *The electrical conductivity of transition metals.* Phys. Rev. Lett., 153:699, 1936. 8

[14] N. F. Mott. *The resistance and thermoelectric properties of the transition metals.* Proc. R. Soc. London, Ser. A, 156:368, 1936. 8

[15] D. Hgele, M. Oestreich, W. W. Rhle, N. Nestle, and K. Eberl. *Spin transport in gaas.* Appl. Phys. Lett., 73:1580, 1998. 8

[16] D. J. Hilton and C. L. Tang. *Optical orientation and femtosecond relaxation of spin-polarized holes in gaas.* Phys.Rev.Lett, 89:146601, 2002. 9, 13, 29

[17] F. Nastos, R. W. Newson, J. Hbner, H. M. van Driel, and J. E. Sipe. *Terahertz emission from ultrafast optical orientation of spins in semiconductors: Experiment and theory.* Phys. Rev. B, 77:195202, 2008. 9, 11, 12, 26, 27, 28, 34, 35, 41, 57, 60, 61

[18] G. Lampel. *Nuclear dynamic polarization by optical electronic saturation and optical pumping in semiconductors.* Phys. Rev. Lett., 20:491, 1968. 9

[19] M. I. Dyakonov and V. I. Perel. *Spin orientation of electrons associated with the interband absorption of light in semiconductors.* Sov. Phys. JETP, 33:1053, 1971. 9, 10, 13, 17

[20] Bernardo S. Mendoza and J. L. Cabellos. *Optical spin injection at semiconductor surfaces.* Phys. Rev. B, 85:165324, 2012. 12

[21] J.G. Braden, J. S. Parke, and P. Xiong. *Direct measurement of the spin polarization of the magnetic semiconductor (ga,mn)as.* Phys. Rev. Lett, 91:5, 2003. 12

[22] Albert W. Overhauser. *Paramagnetic relaxation in metals.* Phys. Rev., 89:689, 1953. 14

[23] R. J. Elliott. *Theory of the effect of spin-orbit coupling on magnetic resonance in some semiconductors.* Phys.Rev., 96:266, 1954. 14, 15

[24] Y. Yafet. *g factors and spin-lattice relaxation of conduction electrons.* Solid State Physics, 14, 1963. 14, 15

[25] M. I. Dyakonov and V. I. Perel. *Spin relaxation of conduction electrons in noncentrosymetric semiconductors.* Sov. Phys. Solid State, 13:3023, 1971. 16, 17, 18

[26] Z. G. Yu and S. Krishnamurthy. *Spin relaxation of electrons and holes in zinc-blende semiconductors*. Phys. Rev. B, 71:245312, 2005. 19, 20, 29

[27] C.A. Schmuttenmaer. *Exploring dynamics in the far-infrared with terahertz spectroscopy*. Chem.Rev., 104:1759, 2004. 23, 38, 40

[28] Ryotaro Inoue, Kazuhisa Takayama, and Masayoshi Tonouchi. *Angular dependence of terahertz emission from semiconductor surfaces photoexcited by femtosecond optical*. J. Opt. Soc. Am. B, 26:9, 2009. 23, 33, 34

[29] X.-C. Zhang and D. H. Auston. *Optoelectronic measurement of semiconductor surfaces and interfaces with femtosecond optics*. J. Appl. Phys., 71:326, 1992. 23, 24, 25, 31

[30] X. C. Zhang, Y. Jin, K. Ware, X. F. Ma, and A. Rice. *Differencefrequency generation and sumfrequency generation near the band gap of zincblende crystals*. Appl. Phys. Lett., 64:622, 1994. 24

[31] M. Bass, P. A. Franken, J. F. Ward, and G. Weinreich. *Optical rectification*. Phys. Rev. Lett., 9:11, 1962. 24

[32] Stefan Schmitt-kink, Benjamin I. Greene, Peter N. Saeta, and Anthony F. J. Levi. *Optical rectification at semiconductor surfaces*. Phys. Rev. Lett., 68:1, 1992. 24

[33] D. Côté, N. Laman, and H. M. van Driel. *Rectification and shift currents in gaas*. Phys. Rev. Lett., 80:905, 2002. 24, 26, 57

[34] M. B. Johnston, D. M. Whittaker, A. Corchia, A. G. Davies, and E. H. Linfield. *Simulation of terahertz generation at semiconductor surfaces*. Phys. Rev. B, 65:165301, 2002. 25, 26, 33, 57

[35] Ping Gu, Masahiko Tani, Shunsuke Kono, Kiyomi Sakai, and X.-C. Zhang. *Study of terahertz radiation from inas and insb*. J. Appl. Phys., 91:5533, 2002. 25, 26

[36] Mark A. Heald and Jerry B. Marion. *Classical Electromagnetic Radiation*. Saunders College Publishing, 1965. 27

[37] M. D. Sturge. *Optical absorption of gallium arsenide between 0.6 and 2.75 ev*. Phys. Rev., 127:768, 1962. 29

[38] X.C. Zhang, B. B. Hu, J. T. Darrow, and D. H. Auston. *Generation of femtosecond electromagnetic pulses from semiconductor surfaces*. Appl. Phys. Lett., 56:1011, 1990. 31

[39] B. B. Hu, X. C. Zhang, and D. H. Auston. *Terahertz radiation induced by subband-gap femtosecond optical excitation of gaas.* Phys. Rev. Lett., 67:2709, 1991. 31, 32, 60

[40] X. C. Zhang, Y. Jin, and X. F. Ma. *Coherent measurement of thz optical rectification from electrooptic crystals.* Appl. Phys. Lett., 61:2764, 1992. 32

[41] F. Nastos and J. E. Sipe. *Optical rectification and shift currents in gaas and gap response: Below and above the band gap.* Phys.Rev. B, 74:035201, 2006. 32

[42] J. E. Sipe and A. I. Shkrebtii. *Second-order optical response in semiconductors.* Phys.Rev. B, 61:5337, 2000. 32, 33, 61

[43] Matthew C. Beard, Gordon M. Turner, and Charles A. Schmuttenmaer. *Terahertz spectroscopy.* J. Phys. Chem. B, 106:7146, 2002. 37

[44] P. R. Smith, D. H. Auston, and M. C. Nuss. *Subpicosecond photoconducting dipole antennas.* IEEE J. Quantum Electron., 24:255. 37

[45] Ch. Fattinger and D. Grischkowsky. *Terahertz beams.* Appl. Phys. Lett., 54:490, 1989. 37

[46] P. Uhd Jepsen, R. H. Jacobsen, and S. R. Keiding. *Generation and detection of terahertz pulses from biased semiconductor antennas.* J. Opt. Soc. Am. B, 13:11, 1996. 37

[47] Yulei Shi, Yuping Yang, Xinlong Xu, Shihua Ma, Wei Yan, and Li Wang. *Ultrafast carrier dynamics in au/gaas interfaces studied by terahertz emission spectroscopy.* Appl. Phys. Lett., 88:161109, 2006. 38

[48] H. Nmec, A. Pashkin, P. Kuel, M. Khazan, and S. Schnll et al. *Carrier dynamics in low-temperature grown gaas studied by terahertz emission spectroscopy.* J. Appl. Phys., 90:1303, 2001. 38

[49] T Hattori, S Arai, R Rungsawang, and K Tukamoto. *Ultrafast intraband electron dynamics of gaas and inp observed by terahertz emission.* Journal of Luminescence, 108:159, 2004. 38

[50] T Hattori, S Arai, and K Tukamoto. *Ultrafast electron dynamics in gaas and inp studied by time-resolved terahertz emission spectroscopy.* Japanese Journal of Applied Physics, 43:7546, 2004. 38

[51] H Ahn, KJ Yu, YL Hong, and S Gwo. *Carrier dynamics of mg-doped indium nitride.* Appl. Phys. Lett., 97:062110, 2010. 38

[52] E Hendry, M Koeberg, JM Schins, LDA Siebbeles, and M Bonn. *Ultrafast charge generation in a semiconducting polymer studied with thz emission spectroscopy.* Phys. Rev. B., 70:033202, 2004. 38

[53] R. A. Smith. *Detectors for ultraviolet, visible, and infrared radiation.* Applied Optics, 4:6, 1965. 39

[54] I : Kasalynas, AJL Adam, TO Klaassen, JN Hovenier, G Pandraud, VP Iordanov, and PM Sarro. *Design and performance of a room-temperature terahertz detection array for real-time imaging.* IEEE JOURNAL OF SELECTED TOPICS IN QUANTUM ELECTRONICS, 14:363, 2008. 39

[55] P Khosropanah, JR Gao, WM Laauwen, M Hajenius, and TM Klapwijk. *Low noise nbn hot electron bolometer mixer at 4.3 thz.* Appl. Phys. Lett., 91:221111, 2007. 39

[56] K Yamashita, A Murata, and M Okuyama. *Miniaturized infrared sensor using silicon diaphragm based on golay cell.* Sensors and actuators A-Physical, 66:29, 1998. 39

[57] Q. Wu and X. C. Zhang. *Freespace electrooptic sampling of terahertz beams.* Appl. Phys. Lett., 67:3523, 1995. 40

[58] Enrique Castro-Camus. *Polarization-resolved terahertz time-domain spectroscopy.* Journal of infrared millimeter and terahertz waves, 33:418, 2012. 40, 42

[59] Nick C. J. van der Valk, Willemine A. M. van der Marel, and Paul C. M. Planken. *Terahertzz polarization imaging.* Optics Letters, 30:2802, 2005. 40

[60] Paul C. M. Planken, Han-Kwang Nienhuys, Huib J. Bakker, and Tom Wenckebach. *Measurement and calculation of the orientation dependence of terahertz pulse detection in znte.* JOSA B, 18:313, 2001. 41

[61] Enrique Castro Camus. *Polarisation resolved terahertz time domain spectroscopy.* PhD thesis, Department of Physics, Condensed Matter Physics, University of Oxford. 41, 43, 44, 45

[62] Enrique Castro Camus. *Polarization-sensitive terahertz detection by multicontact photoconductive receivers.* Appl. Phys. Lett., 86:254102, 2005. 41, 42, 43

[63] E. Castro-Camus, L. Fu, J. Lloyd-Hughes, H. H. Tan, C. Jagadish, and M. B. Johnston. *Photoconductive response correction for detectors of terahertz radiation.* J. Appl. Phys., 104:053113, 2008. 42

[64] A. Hussain and S.R. Andrews. *Title*. Opt. Express, 16:7251, 2008. 42

[65] H. Makabe, Y. Hirota, M. Tani, and M. Hangyo. *Title*. Opt. Express, 15:11650, 2007. 42

[66] E.Castro-Camus, J. Lloyd-Hughes, L. Fu, H.H. Tan, C. Jagadish, and M.B. Johnston. *An ion-implanted inp receiver for polarization resolved terahertz spectroscopy*. Opt. Express, 15:7047, 2007. 43, 44, 45